3-1-2021

Corneal nonmyelinating Schwann cells illuminated by single-cell transcriptomics and visualized by protein biomarkers.

Paola Bargagna-Mohan

Gwendolyn Schultz

Bruce Rheaume

Ephraim F Trakhtenberg

Paul Robson

See next page for additional authors

Authors

Paola Bargagna-Mohan, Gwendolyn Schultz, Bruce Rheaume, Ephraim F Trakhtenberg, Paul Robson, Sonali Pal-Ghosh, Mary Ann Stepp, Katherine S Given, Wendy B Macklin, and Royce Mohan

Received: 13 February 2020 | Revised: 5 October 2020 | Accepted: 25 October 2020

DOI: 10.1002/jnr.24757

RESEARCH ARTICLE

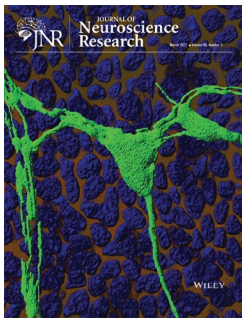

Corneal nonmyelinating Schwann cells illuminated by single-cell transcriptomics and visualized by protein biomarkers

Paola Bargagna-Mohan[1] | Gwendolyn Schultz[1] | Bruce Rheaume[1] | Ephraim F. Trakhtenberg[1] | Paul Robson[2,3] | Sonali Pal-Ghosh[4] | Mary Ann Stepp[4] | Katherine S. Given[5] | Wendy B. Macklin[5] | Royce Mohan[1]

[1]Department of Neuroscience, University of Connecticut Health Center, Farmington, CT, USA

[2]Department of Genetics & Genome Sciences, University of Connecticut Health Center, Farmington, CT, USA

[3]The Jackson Laboratory for Genomic Medicine, Farmington, CT, USA

[4]Department of Anatomy and Regenerative Biology, George Washington University Medical School, Washington, DC, USA

[5]Department of Cell and Developmental Biology, University of Colorado School of Medicine, Aurora, CO, USA

Correspondence
Paola Bargagna-Mohan and Royce Mohan, Department of Neuroscience, University of Connecticut Health Center, 263 Farmington Avenue, Farmington, CT 06030, USA.
Email: bargagna-mohan@uchc.edu (P. B.-M.) and mohan@uchc.edu (R. M.)

Funding information This study was funded, in part, by a UConn Research Excellence Program (REP) stimulus grant to PBM, John A. and Florence Mattern Solomon Endowed Chair in Vision Biology and Eye Diseases fund to RM, National Institutes of Health R01EY029739 grant to EFT, R01EY008512 grant to MAS, and National Institutes of Health R01NS082203 grant to WBM, and Connecticut Innovations grant (16-RMD-UCHC) to PR. The funders had no role in study design, data collection and analysis, decision to publish, or preparation of the manuscript

Abstract

The cornea is the most innervated tissue in the human body. Myelinated axons upon inserting into the peripheral corneal stroma lose their myelin sheaths and continue into the central cornea wrapped by only nonmyelinating corneal Schwann cells (nm-cSCs). This anatomical organization is believed to be important for central vision. Here we employed single-cell RNA sequencing (scRNA-seq), microscopy, and transgenics to characterize these nm-cSCs of the central cornea. Using principal component analysis, uniform manifold approximation and projection, and unsupervised hierarchal cell clustering of scRNA-seq data derived from central corneal cells of male rabbits, we successfully identified several clusters representing different corneal cell types, including a unique cell cluster representing nm-cSCs. To confirm protein expression of cSC genes, we performed cross-species validation, employing corneal whole-mount immunostaining with confocal microscopy in mouse corneas. The expression of several representative proteins of nm-cSCs were validated. As the proteolipid protein 1 (PLP1) gene was also expressed in nm-cSCs, we explored the *Plp1*-eGFP transgenic reporter mouse line to visualize cSCs. Specific and efficient eGFP expression was observed in cSCs in adult mice of different ages. Of several putative cornea-specific SC genes identified, Dickkopf-related protein 1 was shown to be present in nm-cSCs. Taken together, our findings, for the first time, identify important insights and tools toward the study nm-cSCs in isolated tissue and adult animals. We expect that our results will advance the future study of nm-cSCs in applications of nerve repair, and provide a resource for the study of corneal sensory function.

KEYWORDS

cornea, *Plp1*-eGFP transgenic reporter mice, protein biomarkers, RRID:AB_10599115, RRID:AB_1110316, RRID:AB_1849637, RRID:AB_2091333, RRID:AB_2133200, RRID:AB_2313773, RRID:AB_2535855, RRID:AB_2535866, RRID:AB_2633277,

Edited by Dr Aurora Pujol. Reviewed by Anand Swaroop and Judith West-Mays.

RRID:AB_2650603, RRID:AB_570918, RRID:AB_661551, RRID:AB_769875, RRID:AB_844398, RRID:AB_881430, Schwann cells, transcriptome

1 | INTRODUCTION

The transparent cornea helps to focus light onto the neurosensory retina. As the most innervated tissue in the human body (Al-Aqaba et al., 2010; Shaheen et al., 2014), the cornea is distinct, because of its immune privilege and avascularity (Fini & Stramer, 2005; Muller et al., 2003). Myelinated axon bundles that enter the corneal stroma at the periphery lose their myelin sheaths and continue as nonmyelinated axons (Muller et al., 1996, 2003). These axons branch extensively and ascend apically, going through the basement membrane to give rise to leashes that form the subbasal plexus. The subbasal axons then travel anteriorly forming the epithelial nerve plexus and terminate in the superficial layer of the corneal epithelium (He & Bazan, 2016). This anatomical organization preserves a myelin-free axonal network that is important for transparency of the central cornea (Muller et al., 2003).

The Schwann cell (SC) is a specialized glial cell type that ensheaths peripheral nervous system (PNS) axons (Jessen et al., 2008). Two types of SCs can differentiate from their immature progeny. Their fate depends on the types of axons they will ensheath: myelinating SCs (m-SCs) associate in a 1:1 ratio with large caliber axons, whereas a single nonmyelinating SC (nm-SC) ensheaths multiple small caliber axons (<1 μm diameter), forming a structure called the Remak bundle (Feltri et al., 2016; Harty & Monk, 2017). Over the past decades, a vast amount of knowledge has been gained principally on vascularized tissues of the PNS regarding the role of m-SCs in supporting axonal regeneration, including transcriptional responses of SCs to nerve injury (Arthur-Farraj et al., 2017; Clements et al., 2017; Jessen & Mirsky, 2016; Jessen et al., 2015; Napoli et al., 2012). Additionally, single-cell RNA sequencing (scRNA-seq) analysis of the naive uninjured sciatic nerve recently unraveled the targets of nm-SCs that were previously unknown (Wolbert et al., 2020). However, little is known about SCs of the naïve adult mammalian cornea (Muller et al., 1996, 2003), considering also that a recent scRNA-seq analysis of the mouse cornea did not report on these cells (Kaplan et al., 2019). Thus, approaches to characterize corneal SCs (cSCs) need to consider alternate strategies.

Here, we used scRNA-seq analysis to illuminate the global gene expression profile of nm-cSCs, focusing on characterizing this SC subtype from the central cornea of the rabbit, because in area and thickness, the rabbit cornea is similar to that of humans (Ojeda et al., 2001). We anticipated that this low abundance cell population from this corneal tissue could be identified using this powerful approach (Jindal et al., 2018; Mickelsen et al., 2019; Rheaume et al., 2018). We successfully identified a single-cell cluster representing nm-cSC transcripts with distinct markers that distinguished these cells from the other known corneal cell types. The translated proteins for representative SC markers were validated using whole-mount immunostaining in mouse cornea to surmount the challenges of not having validated antibody reagents against the rabbit SC proteins. The WNT signaling inhibitor Dickkopf-related protein 1 (DKK1) is one of the cornea-specific SC genes identified uniquely in the nm-cSC cluster. The cross-species validation endeavor also illuminated another useful SC target, proteolipid protein 1 (PLP1) (Mallon et al., 2002). Exploiting the *Plp1-e*GFP transgenic reporter mouse line, we provide a model for the illumination of the stromal cSC network. In conclusion, our findings have unraveled the distinct features of nm-cSCs, and enabled the development of molecular tools, including a transgenic mouse model, that can be exploited in the future for studying cSCs in corneal physiology and pathobiology.

Significance

Nonmyelinating corneal Schwann cells (nm-cSCs) ensheathing stromal axons in the central aspect of the transparent cornea have not been studied before. Here we used single-cell RNA-sequence analysis of the rabbit cornea and identified several key markers of nm-cSCs, including the novel expression of Dickkopf-related protein 1. Using the proteolipid protein 1 promoter-enhanced green fluorescent protein reporter mouse, we also validated this animal model to study nm-cSCs. These new transcriptomic data, along with several useful tools and reagents we have employed to study nm-cSC functions, should increase our understanding of nm-cSC involvement in injury and disease.

2 | METHODS

2.1 | Animals and corneal harvest

Equal numbers of both female and male C57BL/6 mice (5- to 8-week-old) were used in all experiments. Mice were housed in specific pathogen-free cages in designated laboratory animal housing facilities at UConn Health. Mice were provided enrichment in their cages in the form of plastic cottages and tissue paper. Cages were cleaned two times a week and animals were maintained group housed 4 per cage in an environment of 12-hr dark:light cycles and 66 degree Fahrenheit temperature within 40%–70% humidity. All experiments were conducted in accordance with procedures approved by the Institutional Animal Care and Use Committee (IACUC) of the University of Connecticut Health, and the Association for Research in Vision and Ophthalmology (ARVO) Statement for the Use of Animals in Vision and Ophthalmic Research. Mice were sacrificed by CO_2 inhalation and cervical dislocation. Eyes were immediately enucleated after euthanasia, and corneas were isolated and processed for whole-mount

immunostaining. *Plp1*-eGFP transgenic mice were housed under similar environments on a 14/10 dark:light cycle in designated animal housing facilities under IACUC approved protocols at the University of Colorado School of Medicine. Freshly isolated and snap-frozen eyes from *Plp1*-eGFP transgenic mice aged 2- to 6.5-month(M)-old of both sexes were obtained from Dr. Macklin's laboratory at the University of Colorado School of Medicine (Mallon et al., 2002). The *Plp1*-eGFP transgenic mice have become commercially available (The Jackson Laboratory; Jax Stock#33357; Bar Harbor, ME). New Zealand white rabbits (NCBI:txid9986; 3.2 to 4 kg; male; Envigo, Denver, PA) were housed individually in the Techniplast Caging systems in an AAALACi-accredited facility. The rooms have 12:12 light:dark cycle, average temperature of 66 degrees Fahrenheit, and average humidity of 50%. The rabbits were acclimated for 7 days after arrival. Rabbits were fed a commercial pelleted diet once a day (Teklad 2031, high fiber rabbit diet) and provided acidified-RO water ad-libitum. Rabbit pans were changed three times a week and the cages sanitized every 2 weeks. As part of routine husbandry, rabbit were checked daily, including weekends for clinical well-being. Standard enrichment included toys and food enrichments (three times weekly), such as fruit, vegetables, or hay cubes. Through an arrangement with the donor's laboratory at UConn Health and veterinarian approval, the corneas including an external rim of scleral tissue from eyes of two adult control rabbits were collected within 5 min of rabbit euthanasia. The corneal tissue was placed in ice-cold 1X PBS (140 mM NaCl, 3 mM KCl, 10 mM $NaPO_4$, pH 7.4) solution for subsequent processing.

2.2 | Isolation of corneal cells for scRNA-Seq

The external sclera including a small rim of peripheral cornea was cut using curved scissors to generate corneal buttons (central cornea) following the guidelines from published data on the axial length and radius measurements of the rabbit cornea (Mimura et al., 2008). The endothelium from the corneal buttons was mechanically removed using a pair of forceps and discarded. The corneal buttons were incubated in a 0.25% trypsin solution (ThermoFisher Scientific, Waltham, MA) at 37°C for 30 min to digest the epithelium, which was subsequently removed by gently brushing. The corneal buttons were washed in 1X PBS solution containing 10% fetal bovine serum (FBS), minced into small pieces using scissors, and then incubated in a digestion buffer containing minimal essential medium (MEM; ThermoFisher Scientific, Waltham, MA), 0.03% Dispase II (ThermoFisher Scientific, Waltham, MA), and 0.1% Collagenase type IV (Sigma-Aldrich Corp., St. Louis, MO, USA) at 37°C for 1.5 hr. To break up cell clumps, the cell suspension was gently triturated. An equal volume of MEM containing 10% FBS was added to the digested cell suspension, and cells were filtered through a 20-μm cell strainer (ThermoFisher Scientific, Waltham, MA) and then centrifuged gently. The supernatant was transferred to a new tube and centrifuged again, and a second smaller cell pellet was resuspended and added to the first in ice-cold 1X PBS solution. The final combined cell pellet was resuspended in 100 μl of 1X PBS solution containing 0.05% bovine serum albumin and immediately taken on wet-ice to the Jackson Laboratory (JAX) next door for scRNA-seq analysis.

2.3 | Single-Cell RNA-seq

Cell viability of the corneal cell suspension was assessed on the Countess FL11 at JAX, and found to be high (86%). A representative small portion of the corneal single-cell suspension (targeting ~6,000 cells) was used to load onto the Chromium system (10× Genomics; (Zheng et al., 2017)) for droplet-based single-cell library generation with v3 Chromium chemistry and processed for cDNA library construction and subsequent scRNA-seq analysis (Rheaume et al., 2018). Harvest of corneal tissue through to initiating cDNA synthesis was accomplished in under 3 hr, with cells held on ice where feasible, to minimize transcriptome change. cDNA libraries were sequenced on a Novaseq6000 using the S2 150 cycle kit and targeting to achieve 108,000 reads per cell.

2.4 | Single-cell RNA-seq data analysis

Illumina basecall files (*.bcl) were converted to FASTQs using CellRanger v3.0.1. FASTQ files were then aligned to the rabbit reference genome (OryCun2, version 3.0.2) and transcriptome using the CellRanger v3.0.1 with default parameters, as described in Zheng et al. (2017). A gene filter for downstream analysis retained all genes that had at least two unique molecular identifiers (UMIs) discovered in at least two cells (Figure S1a,b). Gene count data were normalized to total transcripts detected per cell. Briefly, the total UMIs per cell were divided by the count depth of that cell and multiplied by the median count depth of the data set; the result plus a pseudo-count of 1 was then log-transformed. Monocle3 was used for downstream analysis (Qiu, Hill, et al., 2017; Qiu, Mao, et al., 2017; Trapnell et al., 2014). First, a principal component analysis was performed on the normalized data, and variance versus number of principal components (PCs) were plotted (Figure S2). Subsequently, 12 of the PCs explained the majority of the variance in the data and were thus used for dimensionality reduction. The high-dimensional data set was reduced to a three-dimensional (3D) space using a uniform manifold approximation and projection (UMAP) using the default Monocle3 parameters. Clusters were assigned in an unbiased manner using Monocle3's cluster_cells function with default parameters. The dimensionality reduction and subsequent clustering resulted in four molecularly distinct clusters. After identifying the cSC cluster, all further downstream analyses were performed on this cSC cluster alone.

2.5 | Mouse cornea preparation for whole-mount immunostaining

Mouse corneas were briefly washed in 1X PBS solution and endothelium and epithelium were carefully removed, as previously described (Fini et al., 1998). A small area of epithelium was left intact at the limbus/periphery to facilitate the orientation of the corneas prior to confocal

imaging. After a brief wash with 1X PBS solution to remove debris, four incisions were made in each cornea, and tissues were fixed in fresh 4% paraformaldehyde (PFA) for 1 hr at room temperature, followed by one wash with 1X PBS solution containing 1% Triton-X, and two washes with 1X PBS solution for 30 min each. Corneas were then blocked, and permeabilized in 1X PBS solution containing 0.5% Triton-X, 5% goat serum, and 1% BSA for 1 hr at 37°C, and then 48 hr at 4°C. Primary antibodies were diluted in a DAKO background-reducing medium (Cat # S3022, Aligen, Santa Clara, CA), and corneas were incubated for 1 hr at 37°C, and then 48 hr at 4°C. After one wash with 1X PBS solution containing 1% Triton-X and two washes with 1X PBS solution for 30 min each, tissues were incubated with appropriated secondary antibody (Table 1) in a DAKO background-reducing medium for 1 hr at 37°C, and then overnight at 4°C. The following day, corneas were washed once with 1X PBS solution containing 1% Triton-X for 1 hr, followed by two washes with 1X PBS solution for 30 min each. Nuclei were stained with 4′,6-diamidino-2-phenylindole (DAPI) for 10 min. The corneas were cover-slipped with an anti-fading mounting media, and analyzed by epi-fluorescence or confocal microscopy. Primary and secondary antibodies with their corresponding Research Resource Identifiers (RRID) and the dilutions used in this study are listed in Table 1.

2.6 | Microscopy

Whole mounts of mouse corneas were examined by epifluorescence microscopy using an inverted Olympus IX81 microscope to initially determine the quality of immunostaining. These slides were

TABLE 1 Primary and secondary antibodies used in immunofluorescence studies

Antibody name	Dilution	Vendor and catalog #RRIDs	Clonality	Host
Anti-SOX10 antibody	1:100	Abcam Cat# ab155279 RRID:AB_2650603	Monoclonal	Rabbit
Anti-Murine SCN7A	1:100	Novus Cat# NB100-81029 RRID:AB_1110316	Polyclonal	Rabbit
Anti-Neural Cell Adhesion Molecule L1 clone 324	1:200	Millipore Cat#MAB5272 RRID:AB_2133200	Monoclonal	Rat
Anti-Myelin Basic Protein	1:200	Abcam Cat# 218011 [EPR21188]	Monoclonal	Rabbit
Anti-βIII-Tubulin	1:200	Biolegend Cat# 801201 RRID:AB_2313773	N/A	Mouse
Anti-βIII-Tubulin	1:200	Millipore Cat# AB9354 RRID:AB_570918	Polyclonal	Chicken
Anti-PLP1 (ab1)	1:200	Sigma Cat#SAB2101830 RRID:AB_10599115	Polyclonal	Rabbit
Anti-GFRalpha3	1:100	Sigma Cat#PRS1137 RRID:AB_1849637	Polyclonal	Rabbit
Anti-type VII Collagen	1:200	Immundiagnostik Cat# AL1002.4 RRID:AB_769875	N/A	Rabbit
Anti-Myelin Protein Zero	1:200	Abcam Cat#39375 RRID:AB_881430	Polyclonal	Chicken
Anti-Syndecan-3 (D-19)	1:200	Santacruz Cat# sc-9496 RRID:AB_661551	Polyclonal	Goat
Anti-DKK1	1:100	Abcam Cat#ab61034 RRID:AB_2091333	Polyclonal	Rabbit
Goat anti-Chicken IgY (H + L) Alexa Fluor 647	1:300	Thermo Fisher Scientific Cat# A-21449 RRID:AB_2535866	Polyclonal	Goat
Goat anti-Rabbit IgG (H + L), DyLight 488	1:500	Thermo Fisher Scientific Cat# 35552 RRID:AB_844398	Polyclonal	Goat
Goat anti-Rat IgG (H + L) Cross-Adsorbed Secondary Antibody, Alexa Fluor 555	1:300	Thermo Fisher Scientific Cat# A-21434 RRID:AB_2535855	Polyclonal	Goat
Goat anti-mouse (H + L) Secondary	1:300	Thermo Fisher Scientific Cat# A-32728 RRID:AB_2633277	Polyclonal	Goat

then subjected to confocal microscopy (Zeiss LSM-880) provided by the CCAM Microscopy Facility at UConn Health. The confocal is mounted on an inverted Axio Observer Z1. The 880 employs the spectral 32-channel QUASAR GaAsp detector allowing for spectral imaging, maximum sensitivity photon counting, and two adjacent PMT's. *z*-stack images were acquired at different magnifications and compacted into one maximum intensity projection (MIP) image after alignment. All adjustments on brightness/contrast were made while still maintaining the original ratio of the wavelengths used (FICT, TRICT, CY5). Zen Blue software (Carl Zeiss, Inc.), provided by the CCAM Microscopy Facility at UConn Health, was used to perform 3D reconstruction, MIP, and orthogonal reconstruction.

2.7 | Transmission electron microscopy

Corneas of adult C57BL/6 mice were fixed and processed for scanning and transmission electron microscopy as previously described (Bargagna-Mohan et al., 2017).

2.8 | Statistics, rigor, and reproducibility

The scRNA-seq data represents corneal cells that were pooled from four corneas derived from two male adult rabbits. Only a small representative fraction of cells from this mixed pool of cells was employed for scRNA-seq analysis. Mouse corneal tissue for whole-mount immunostaining experiments were performed using eyes of different batches of wild-type C57BL/6 mice (n = 4/immunostaining experiment) with the inclusion of both sexes; a total of 32 C57BL/6 mice were employed. Eyes from *Plp1*-eGFP mice (n = 3 mice/age group) were also employed to ensure sufficient coverage of adult stages; a total of nine *Plp1*-eGFP mice were employed. Investigators were blinded to the sex of mice during processing of tissue and image analysis.

3 | RESULTS

3.1 | scRNA-seq analysis of the rabbit cornea

Initial pilot studies failed to isolate high yields of viable cSCs from the mouse cornea. Hence, the rabbit cornea became a viable option as we could coordinate the scRNA-seq analysis with the timing of isolation of sufficient volumes of fresh corneas in this model (see Methods). The workflow of steps undertaken for this analysis is represented in Figure 1a. The data after filtering provided us a total of 6,546 cells for analysis, resulting in a median of 9,195 UMIs per cell and a median of 2,066 genes per cell. The single-cell transcriptomes from these corneal cells were then subjected to unsupervised clustering. Clusters were called based on positions in the 3D space of the UMAP projection leading to a profile of four distinct cell clusters. The differentially expressed genes (DEGs) between clusters were used to identify the cell type that the clusters represented (Figure 1b). This allowed us to annotate the four cell clusters as: corneal keratocytes, epithelial cells, dendritic cells/macrophages, and nm-cSCs based on known markers for each cell type (Figure 1c).

As anticipated, we found corneal keratocytes to be the most abundant cell type (69.4%) of the cornea (Figure 1b), considering that the bulk of the relatively thick corneal stroma is populated by these resident cells. The top DEGs of the keratocyte cluster include type I collagen (*COL1A1*, *COL1A2*), thrombospondin-2 (*THBS2*), syndecan-2 (*SDC2*), alpha-2-microglobulin (*A2M*), and platelet-derived growth factor receptor-like protein (*PDGFRL*) (Bi & Lwigale, 2019) (Figure 1c). The epithelial cell cluster (29.7%) showed prominent expression of transcripts for keratin 3 (*KRT3*), desmoplakin (*DSP*), aquaporin 3 (*AQP3*), and transcription factor Pax6 (*PAX6*) (Figure 1c) (You et al., 2018). These epithelial cells were invariably included due to incomplete removal of the epithelium prior to stromal digestion. However, successful elimination of limbal tissue and conjunctiva was achieved as transcripts for keratins (*KRT15*, *KRT13*) and the mucin, *MUC4*, that define limbal-conjunctival cells (Geisert et al., 2009), were not detected. A smaller cell cluster (0.52%) representing a mixture of tissue-resident macrophages and dendritic cells expressed transcripts for *AIF1*, *HLA-DMA*, *RLA-DR-ALPHA*, and *CD74* (Figure 1c). Lastly, the nm-cSC cluster (0.44%) contained several SC-marker transcripts (*SCN7A*, *COL3A1*, *SOX10*, *GFRA3*, *CDH19*, *PMP22*, and *CNMD*) that were abundantly expressed (see also next section) (Arthur-Farraj et al., 2012; Franzen et al., 2019; Monje et al., 2018). We did not anticipate a corneal endothelial cell cluster as this tissue layer was completely peeled off prior to tissue digestion. Indeed, transcripts for endothelial cell markers *COL8A2*, *SLC4A11*, and *CYYR1* (Chng et al., 2013) were not found. The expression of additional cell type markers for keratocytes, epithelial cells, and macrophages/dendritic cells are shown (Figure 1d). As we were able to identify nm-cSCs by several known markers, the interrogation of the other corneal cell clusters was not pursued further here, but will be included in a more detailed study to follow.

3.2 | nm-cSCs express many known conserved SC markers

There were a total of 29 cells in the cluster we defined as nm-cSC with median UMI of 2,233.5 and 1,142.5 median genes per cell, and a total of 65,332 unique mRNA molecules and 6,057 genes detected across this cluster, thus a suitable representation of the nm-cSC transcriptome. The top 50 DEGs in the nm-cSC cluster, as reflected by their SC specificity (Figure 2a), were assessed by interrogating the literature and relevant databases *PanglaoDB* (Arthur-Farraj et al., 2012; Franzen et al., 2019; Monje et al., 2018; Wolbert et al., 2020) and *Harmonizome* (Rouillard et al., 2016). The *SCN7A* transcript, a marker of nm-cSCs was abundantly expressed in all the 29 cells of the cluster. As anticipated, transcripts of m-SCs were not found in this cluster consistent with the removal of myelinated tissues (see Methods). This is evidenced by our failure to detect any of

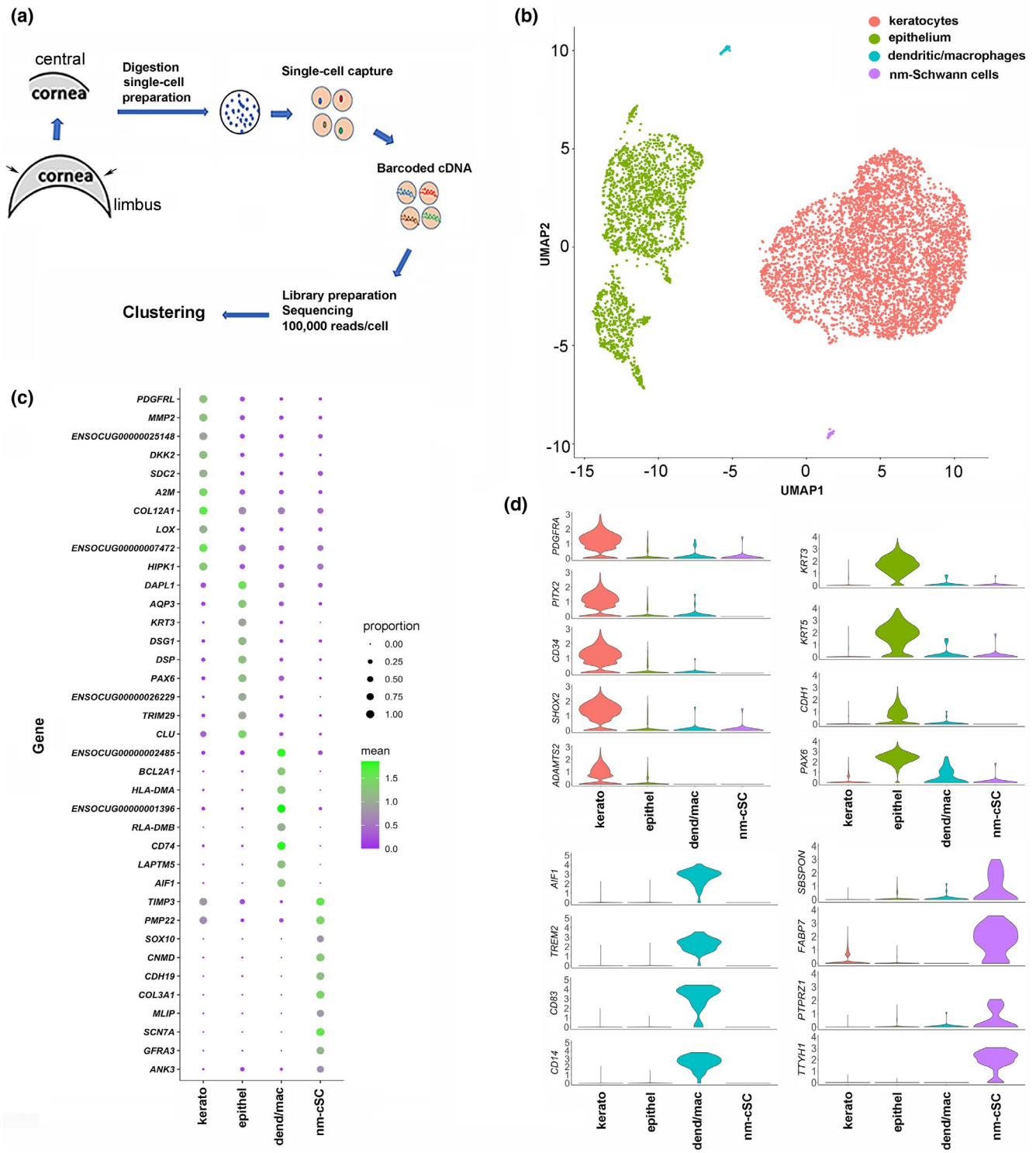

FIGURE 1 scRNA-seq analysis of rabbit corneas. (a) Outline of experimental procedures for the endothelial cell-depleted central corneal cell preparation for scRNA-seq analysis. (b) Major corneal cell populations were identified by unsupervised clustering. Each dot represents a single cell that was designated by color of the cluster. The high-dimensional data set was reduced to a three-dimensional space using a uniform manifold approximation and projection (UMAP) and default Monocle3 parameters. (c) The dot plot identifies the major cell types by marker gene expression. The size of the dots reflect the proportion of cells of each cell type expressing the marker gene and the intensity of color reflects the mean expression of each marker gene across all the cells. (d) Violin plots, representing the distribution of log-transformed normalized gene expression (gene UMIs/total UMIs) for markers in each cluster. Kerato = keratocytes, epithel = epithelium, dend/mac = dendritic cells/macrophages, nm-cSC = nonmyelinating corneal Schwann cells [Color figure can be viewed at wileyonlinelibrary.com]

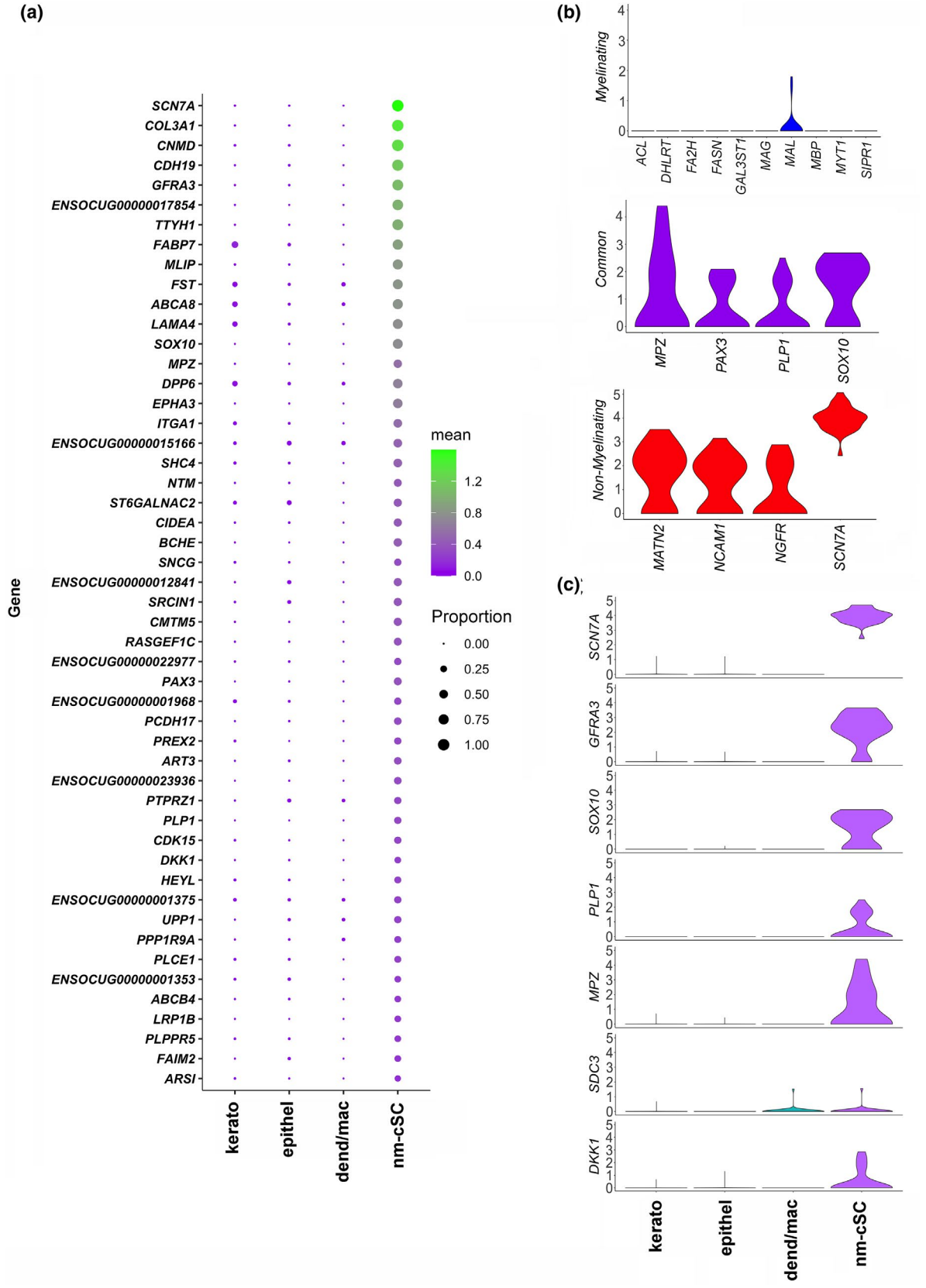

FIGURE 2 The major transcripts of corneal nonmyelinating SCs. (a) Top 50 differentially expressed genes in the nm-cSC cluster represent many conserved SC markers. (b) Violin plots, representing the distribution of log-transformed normalized gene expression (gene UMIs/total UMIs) for marker expression of nonmyelinating SCs, myelinating SCs, and SC markers commonly expressed in both cell types. (c) Violin plots, representing the distribution of log-transformed normalized gene expression across all cells for SC markers selected for validation in mouse corneas. Kerato = keratocytes, epithel = epithelium, dend/mac = dendritic cells/macrophages, nm-cSC = nonmyelinating corneal Schwann cells [Color figure can be viewed at wileyonlinelibrary.com]

the major myelination gene transcripts, including *MBP*, *MAG*, the myelin transcription factor (*MYT1)*, or transcripts for proteins involved with myelin lipid metabolism, such as, *ACL*, *FASN*, *DHCR7*, *GAL3ST1*, *FA2H*, and *S1PR1* (Figure 2b) (Monje et al., 2018). Expression of *MATN2*, *NGFR*, and *NCAM1* transcripts further confirmed this corneal cluster contains only nm-SCs (Figure 2b). Along with *SOX10* (Bremer et al., 2011), SC transcripts commonly expressed by both m-SCs and nm-SCs (*GFRA3*, *COL3A1*, *CDH19*, *PAX3*, *ART3*, *CNMD*, *PLP1*, *FABP7*, *MLIP*, *CD9*, and *TTYH1)* were found (Figure 2a,b) (Arthur-Farraj et al., 2017; Franzen et al., 2019; Monje et al., 2018). *PAX3* was expressed in many of the nm-cSCs revealing their identity as mature nm-cSCs (Blake & Ziman, 2013; Jessen & Mirsky, 2016). Altogether, nm-cSCs are of low abundance in the central cornea; however, with the inclusion of m-cSCs and nm-cSCs contained in the peripheral cornea, the total number of cSCs could possibly reach 1%, as seen in the dermis (Guerrero-Juarez et al., 2019).

3.3 | Identification of multiple biomarkers of cSCs

We performed cross-species validation for representative rabbit nm-cSC targets using adult mouse corneas to circumnavigate the scarcity of reputable antibodies against rabbit antigens. This also gave us the advantage with the thinner mouse tissue to illuminate the 3D structures of cSCs by confocal microscopy (He & Bazan, 2016; Stepp, Pal-Ghosh, Tadvalkar, Williams, et al., 2018). To initially map the stromal axonal network of the mouse cornea, whole corneas were immunostained for the neuronal-specific marker βIII-tubulin (Figure 3a). This allowed us to visualize the entire corneal stromal network, revealing several branching patterns. Some axonal trunks divided and terminated near the central cornea (Figure 3a, red dotted line), others spanned limbus-to-limbus and interconnected with each other (Figure 3a, white dotted line). The density of stromal nerves was higher in the periphery than in the central cornea, as previously reported (Yang et al., 2018). Transmission electron microscopy (TEM) analysis showed the presence of myelinated and nonmyelinated (Figure 3b) axonal fibers at the limbal/peripheral area, whereas, in the central cornea a single nm-cSC ensheathed multiple nonmyelinated axons (Figure 3c). Often, stromal resident cells, namely keratocytes, were noted in close proximity to the nerve bundles (Figure 3c).

We investigated the stromal expression of the nm-SC marker L1CAM (Schmid et al., 2000), as studies in mice revealed that L1CAM expression in corneal epithelial cells may promote cell–cell interactions between the axon terminals and epithelial cells (Stepp, Pal-Ghosh, Tadvalkar, Li, et al., 2018; Stepp et al., 2017). To reduce background staining, the epithelium was removed, and only a small portion of the subbasal plexus was preserved at the limbus for tissue orientation during confocal microscopy. As shown in Figure 4a, βIII-tubulin immunostained all the stromal nerve fibers radially derived from thick limbal axons that run toward the central cornea forming the subepithelial stromal nerve plexus. L1CAM expression followed the branching pattern of these axons (Figure 4a). In the stroma some axonal branches, mostly in the central cornea, were not fully enveloped by L1CAM$^+$ cells (Figure 4b). L1CAM immunostaining in nm-cSCs was more evident at the limbus/periphery,

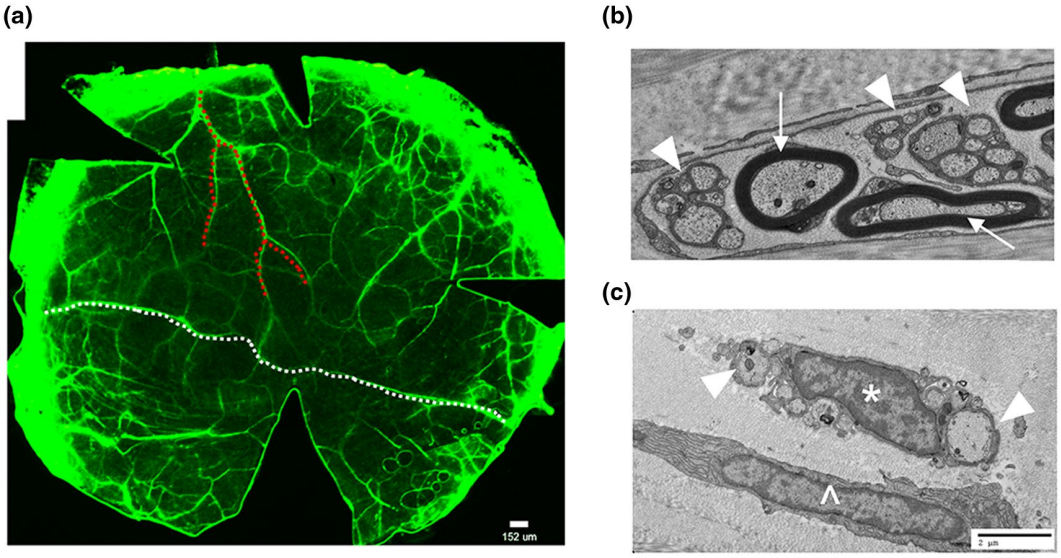

FIGURE 3 Visualization of axons and Schwann cells in the cornea. (a) Representative image of a whole-mount mouse cornea immunostained for βIII-tubulin (*green*) to demark the innervation network in the stroma. The epithelium was removed to reduce background staining. Two separate images were stitched together using Adobe Photoshop. The corneal nerves show several branching patterns; some trunks divide and terminate near the central cornea (*red dotted line*), others span limbus-to-limbus and interconnect with each other (*white-dotted line*). Scale bar, 152 μm (b) Transmission electron microscopy of mouse corneas showing myelinated (*thin arrows*) and nonmyelinated (*arrow heads*) nerve fibers in the limbal area. (c) Transmission electron microscopy of a mouse cornea showing a nonmyelinated nerve fiber (*arrow heads*) in the central cornea. The asterisk demarks the nucleus of an nm-SC, which is in close proximity to a keratocyte (*caret*). Scale bar, 2 μm.*n* = 4 corneas [Color figure can be viewed at wileyonlinelibrary.com]

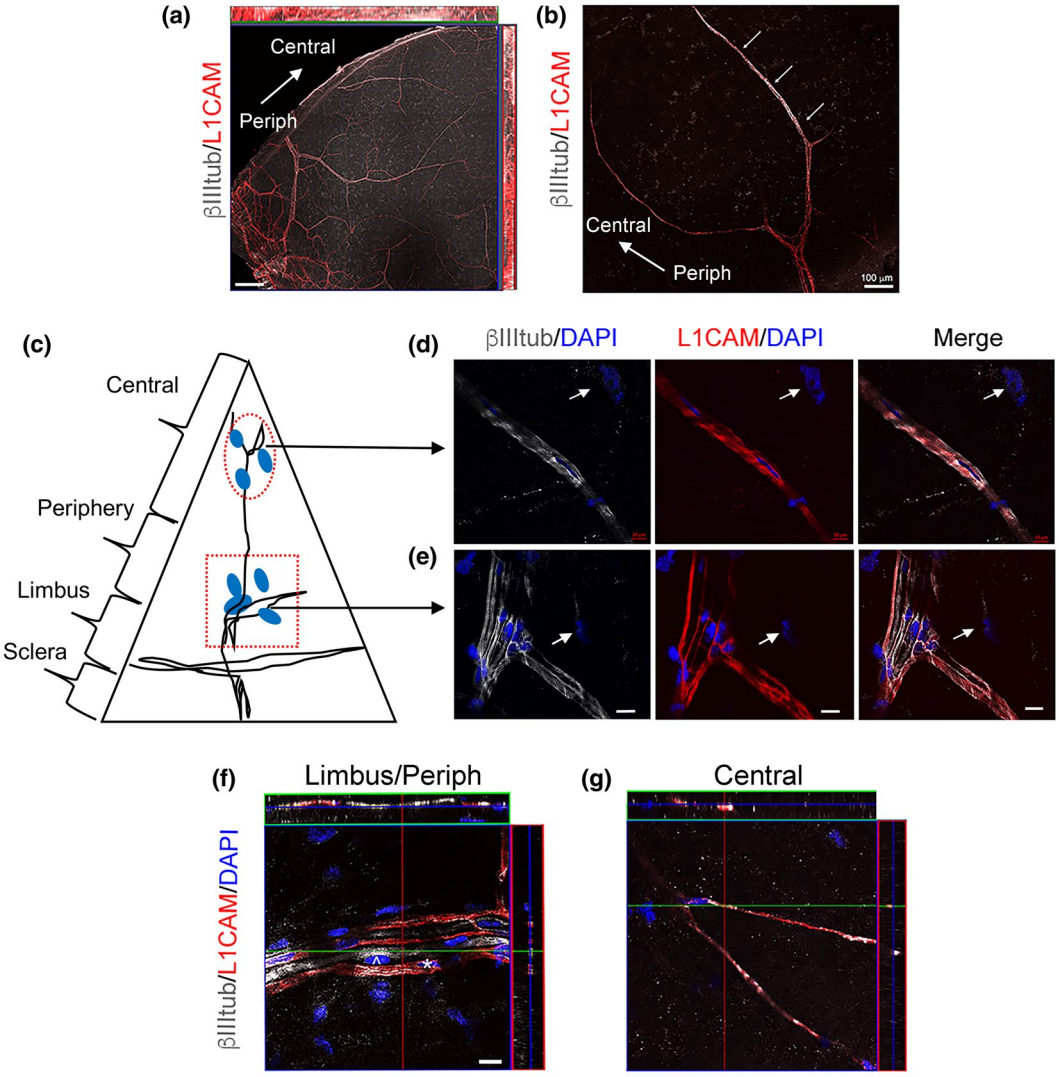

FIGURE 4 L1CAM is a marker of nm-cSCs. Mouse corneas ($n = 4$) were immunostained as whole mounts for L1CAM (*red*) and βIII-tubulin (*gray*) expression. (a) Maximal intensity projection (MIP) ofz-stacks taken from the subbasal plexus toward the deep stroma. (b) Representative confocal image at low magnification (20×) of stromal axons immunostained for βIII-tubulin (*gray*) branching from the limbal/peripheral area to the central cornea, and co-immunostained for L1CAM (*red*).*Thin arrows*demark axons with less intense L1CAM immunostaining. Scale bar, 100 μm. (c) Representative confocal image at high magnification (63×) of stromal axons immunostained for βIII-tubulin (*gray*) at the limbal/peripheral cornea. L1CAM$^+$cells (*red*) overlapped only with selective βIII-tubulin$^+$axons (*gray*).*Arrows*point to the nucleus of a L1CAM$^-$cell. Scale bar, 10 μm. (d) Representative confocal image at high magnification (63×) of stromal nerves in the central cornea.*Arrows*point to the nucleus of a L1CAM$^-$cell. Scale bar, 10 μm. Orthogonal views from different planes (x/y,x/z, ory/z) of merged confocal images at the limbal/peripheral cornea (f), and in the central cornea (g).*Asterisk*demarks the nucleus of an L1CAM$^+$cell (*red*), and*caret*demarks the nucleus of a cell immunostained only with βIII-tubulin (*gray*). Scale bar, 10 μm. Nuclei were stained with DAPI (*blue*). βIIItub = βIII-tubulin [Color figure can be viewed at wileyonlinelibrary.com]

where L1CAM$^+$ cells selectively ensheathed nonmyelinated βIII-tubulin$^+$ axons (Figure 4e,f), as the myelinated axons (MBP$^+$ and MPZ$^+$; Figure S3a,b) did not co-immunostain with L1CAM$^+$ cells. In the central cornea, L1CAM$^+$ nm-cSCs enveloped βIII-tubulin$^+$ axons (Figure 4d,g), and nearby cells, namely resident stromal keratocytes, were L1CAM negative (Figure 4d). Interestingly, *L1CAM* transcripts were not found in the nm-cSC cluster from the rabbit cornea, suggesting that this gene may be regulated in a species-specific manner.

Next we selected representative genes that have important physiological roles with high and moderate transcript expression levels from the top 50 DEGs in the nm-cSC cluster (Figure 2a). Both SCN7A and GFRA3 are expressed in nm-SCs (Franzen et al., 2019). As shown in Figure 5, SCN7A co-localized with L1CAM in the central cornea (Figure 5b-iii), as well at the limbal/peripheral zone (Figure 5c-iii). In particular, L1CAM$^+$ and SCN7A$^+$ nm-cSCs wrapped around both stromal (Figure 5b, dotted arrows) and subbasal axons (Figure 5b, arrows). This was more evident using a 3D reconstruction (Figure 5e), where only nm-cSCs immunostained for L1CAM and SCN7A, as resident keratocytes, were negative for both antibodies (Figure 5d,e, asterisks). Immunostaining for GFRA3 and L1CAM (Figure 6) also revealed a high degree of co-localization around

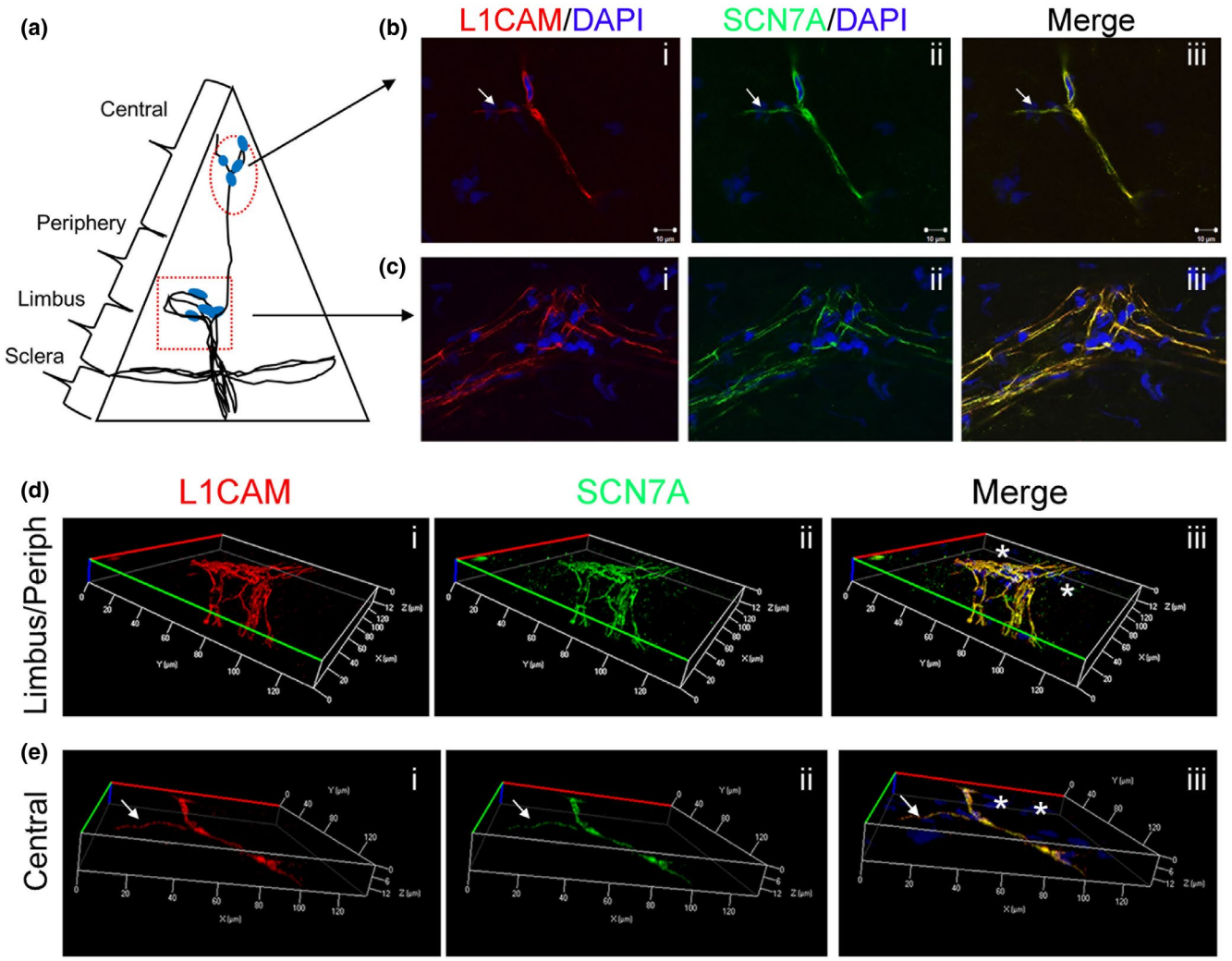

FIGURE 5 Visualization of SCN7A expression in cSCs. (a) Schematic representation of the cornea mapping the distribution of stromal axons and cSCs. Representative confocal images of stromal cSCs immunostained for SCN7A (*green*), L1CAM (*red*) were taken in (b) from the central cornea (*dotted circle)*, and at the limbal/peripheral area (*dotted rectangle*) in (c). A strong co-localization of L1CAM with SCN7A (*yellow*) was noted. Scale bars, 10 μm. 3D reconstruction of 12 μmz-stacks acquired at the limbal/peripheral area (d), and 16 μmz-stacks acquired in the central portion of the cornea (e). A*sterisks*demark nuclei of corneal resident cells, namely keratocytes. SCN7A = Sodium channel, voltage-gated, type VII, alpha subunit. Nuclei were stained with DAPI (*blue).n* = 4 corneas [Color figure can be viewed at wileyonlinelibrary.com]

the stromal nerves; however, the immunostaining pattern of GFRA3 appeared to be absent in some stromal areas (Figure 6b, dotted arrows) and in the cSCs wrapping the subbasal axons (Figure 6b solid arrows). An orthogonal MIP view of images in Figure 6b revealed that GFRA3$^+$ nm-cSCs were indeed wrapping the stromal axons, but GFRA3 immunostaining was absent around the subbasal axons (Figure 6c, solid arrows). As shown in Figure 7, SOX10 was immunolocalized in the mouse corneas. In the central stroma, SOX10 was restricted to the nuclei of nm-cSCs L1CAM$^+$ (Figure 7b, asterisks), whereas at the corneal periphery SOX10 immunostained the nuclei of both m-cSCs (Figure 7c, carretts) and nm-cSCs (Figure 7c, asterisks). Several SOX10-negative nuclei of resident keratocytes were also noticed in proximity of the axons (Figure 7b,c, arrows), as supported by our TEM findings (Figure 1d).

We then investigated the expression of syndecan-3 (SDC3) as previous studies documented its expression on intraepithelial corneal nerves (ICNs) (Pal-Ghosh et al., 2017). ICNs and stromal nerves were both positive for βIII-tubulin (Figure 8c), and SDC3 immunostaining was more intense in the ICNs compared to stromal nerves (Figure 8b). Stromal nerves were surrounded by SDC3$^+$ nm-cSCs (Figure 8b,e); however, after nerves penetrated the basement membrane (BM), forcing the COL7 aside (Figure 8f), SDC3 expression was lost. This finding revealed that in the corneal stroma SDC3 is restricted to cSCs. Interestingly, *SDC3* transcripts were expressed at very low levels in the rabbit nm-cSC cluster (Figure 2c). This suggests that *SDC3* may be possibly regulated in a species-related manner in the cornea.

The proteolipid protein 1 (PLP1), a major component of myelin, is also found in nm-SCs (Wight et al., 1993). Immunostaining for PLP1 and L1CAM revealed a high degree of co-localization around the stromal nerves, both in the central (Figure 9b) and peripheral areas (Figure 9c). In the periphery cross-sectional view of the same image in Figure 9c, PLP1 co-localized with L1CAM$^+$ nm-cSCs, but also wraps around βIII-tubulin$^+$ axons negative for L1CAM (Figure 9d). In the central cornea PLP1

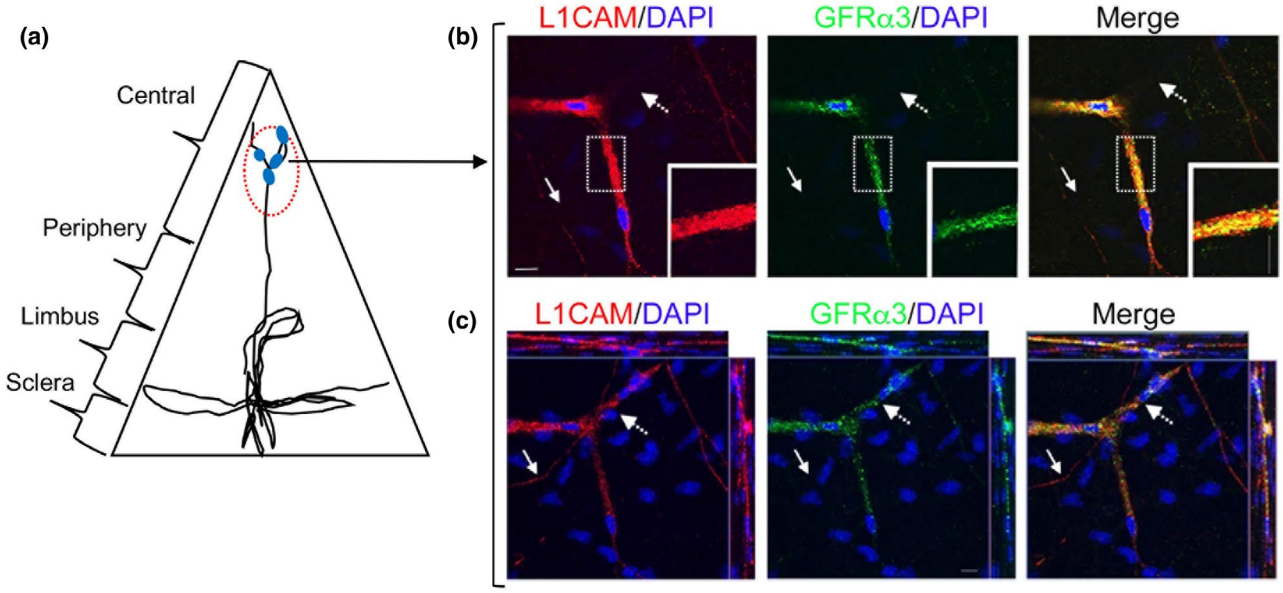

FIGURE 6 Visualization of GFRA3 expression in cSCs. (a) Schematic representation of the cornea mapping the distribution of stromal axons and cSCs. Representative confocal images of stromal cSCs immunostained for L1CAM (*red*), GFRA3 (*green*) were taken in (b) from the central cornea (*dotted circle).Insertsin* (b):images of stromal nm-cSCs were enlarged 5×. To be noted that co-localization of L1CAM with GFRA3 (*yellow*) appeared punctate. Scale bars, 10 μm. (c) Orthogonal views from different planes (*x*/*y*,*x*/*z*, or*y*/*z*) of merged confocal images from (b). Co-localization of L1CAM (*red*) with GFRA3 (*green*) was dotted, and GFRA3 immunostaining was absent in the subbasal plexus (*arrows*), compared to the deeper stroma (*dotted arrows*). All images were taken at 63× magnification; Scale bars, 10 μm. Nuclei were stained with DAPI (*blue).* GFRA3 = GDNF family receptor alpha-3.*n* = 4 corneas [Color figure can be viewed at wileyonlinelibrary.com]

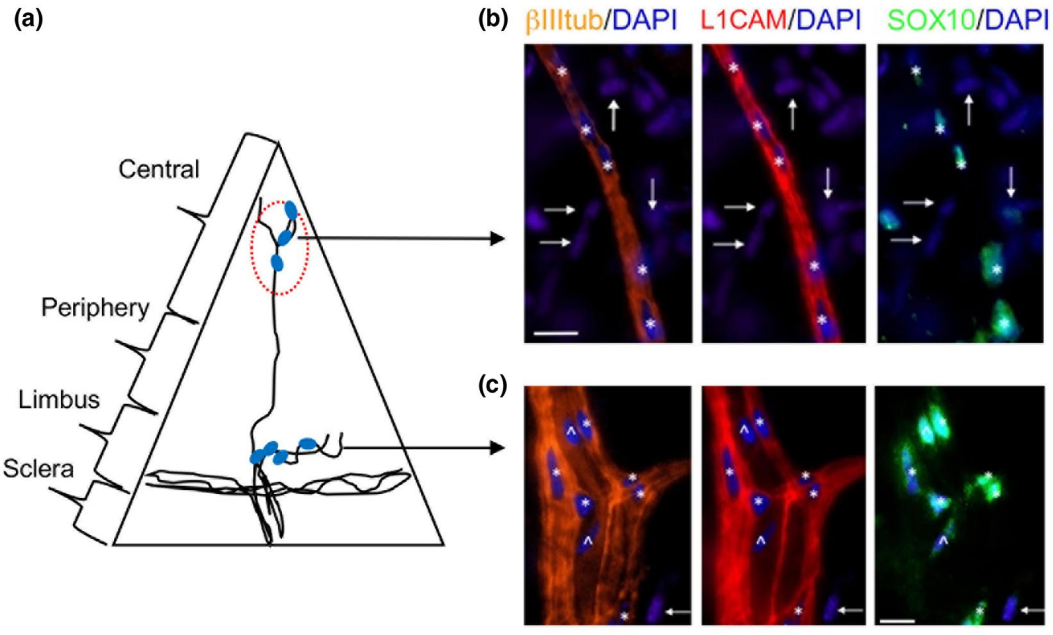

FIGURE 7 Visualization of SOX10 expression in cSCs. (a) Schematic representation of the cornea mapping the distribution of stromal axons. Representative epifluorescence images of stromal axons and cSCs immunostained for L1CAM (*red*), SOX10 (*green*), and βIII-tubulin (*orange*) were taken in (b) from the central cornea (*dotted circle),* and in (c) at the limbal/peripheral area (*dotted rectangle*).*Asterisks*indicate nuclei of L1CAM$^+$cells, and*caretsd*emark the nuclei of L1CAM$^-$cells, most likely m-cSCs.*Arrows*indicate the nuclei of other corneal resident cells, most likely keratocytes. Images were taken at 40× magnification. Scale bars, 10 μm. Nuclei were stained with DAPI (*blue).n* = 4 corneas [Color figure can be viewed at wileyonlinelibrary.com]

co-localized with L1CAM$^+$ nm-cSCs (Figure 9e), suggesting that nm-cSCs in the central cornea express PLP1 protein. Given these results, we then assessed whether the *Plp1-eGFP* transgenic mouse (Buchstaller et al., 2004) could serve as a model to visualize cSCs. The corneas of *Plp1-eGFP* mice showed retention of eGFP fluorescence signal after tissue fixation at 4 M post-birth (Figure 10a), and we confirmed that eGFP$^+$

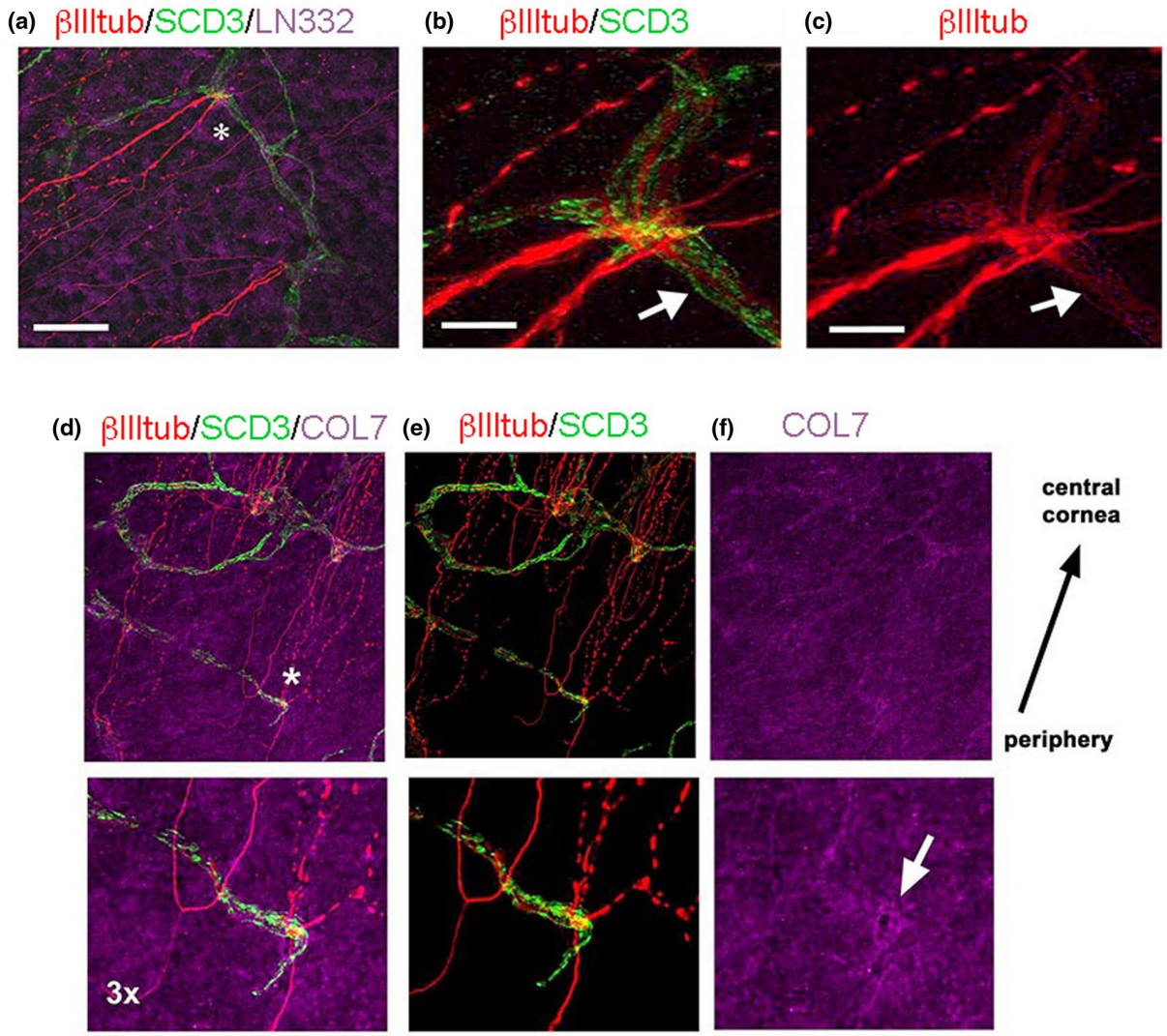

FIGURE 8 Visualization of syndecan-3 expression in cSCs.*En face*extended focus projection confocal image showing corneal epithelium projected from the basal aspect of the tissue at the level of the corneal epithelial basement membrane. All representative images ($n = 3$ corneas) were acquired at the corneal periphery. (a) Corneal epithelium immunostained for βIII-tubulin (*red*), syndecan-3 (SDC3;*green*), and laminin 332 (LN322,*magenta*), a basement membrane component. Asterisk demarks an area magnified 3×, presented in B and C. (b) Enlarged image showing βIII-tubulin and SDC3 immunostaining, and (c) βIII-tubulin alone to demonstrate that stromal nerves were also βIII-tubulin$^+$. Bar in A = 26 μm; bars in B and C = 8.7 μm. (d) Corneal epithelium immunostained for βIII-tubulin (*red*), syndecan-3 (SDC3;*green*), and Collagen 7 (COL7,*magenta*). Asterisk demarks an area magnified 3×, presented in E and F.*Arrow*shows where the stromal nerves penetrate the basement membrane forcing the Col7 aside. Bars = 32 μm [Color figure can be viewed at wileyonlinelibrary.com]

cells labeled the nm-cSCs by co-immunostaining for L1CAM using 2 M (Figure 10b), and 6.5 M-old corneas (Figure 10c). Transgenic corneas co-immunostained for LICAM and examined at different stromal depths (Figure S4) and across the stroma (Figure S5) revealed marked overlap in detection of SCs in both these directions. These results confirmed that the *Plp1* gene promoter has specificity for cSCs.

3.4 | Novel cornea-specific expression of DKK1 in nm-SCs

From our scRNA-seq analysis, several transcripts in the nm-cSC cluster (*DPP6*, *ST6GALNAC2*, *CIDEA*, *CDK15*, *DKK1*, *ABCB4*, *LRP1B*, *PLPPR5*) were novel to this cell type (Arthur-Farraj et al., 2012; Franzen et al., 2019; Monje et al., 2018; Rouillard et al., 2016; Wolbert et al., 2020). In particular, DKK1 is especially interesting, because this WNT inhibitor (Ahn et al., 2011) plays a role in eye development and anterior segment homeostasis (Benson et al., 2017; Lieven & Ruther, 2011; Nakatsu et al., 2011). To investigate whether DKK1 protein is expressed in the murine cSCs, we immunostained adult *Plp1-eGFP* mouse corneas with anti-DKK1 antibodies. Expression of DKK1 was found overlapping with eGFP + SCs in both central (Figure 11b) and peripheral areas (Figure 11c) of the cornea. This finding identifies, for the first time, that DKK1 is expressed in a cSC-specific manner and confirms the cross-species expression of this important WNT signaling inhibitor protein.

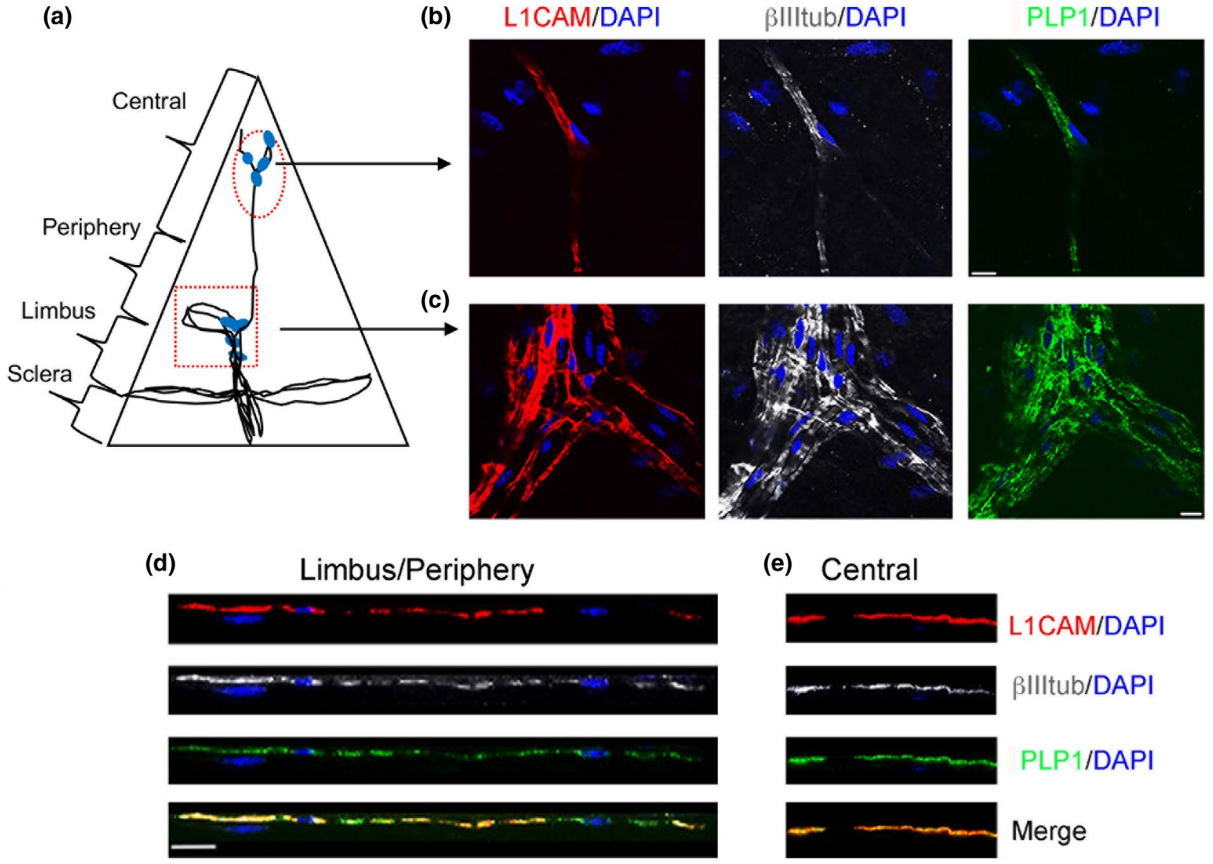

FIGURE 9 Visualization of PLP1 expression in cSCs. (a) Schematic representation of the cornea ($n = 4$) mapping the distribution of stromal axons. Representative confocal images of stromal axons and cSCs immunostained for L1CAM (*red*),*PLP*1 (*green*), and βIII-tubulin (*gray*) were taken in (b) from the central cornea (*dotted circle*), and in (c) at the limbal/peripheral area (*dotted rectangle*). (d, e) Sagittal views ofz-stacks of the same image in (b) and (c). To be noted that PLP1 co-localized with L1CAM^{+}nm-cSCs (*yellow*). (f) 3D reconstruction of 12 μmz-stacks acquired in the central portion of the cornea. Strong co-localization between L1CAM and PLP1 (*yellow*) was noted. Numerous nuclei of resident cells, namely keratocytes, surrounded the stromal nm-cSCs. All images were taken at 63× magnification; Scale bars, 10 μm. PLP1 = proteolipid protein 1. Nuclei were stained with DAPI (*blue*) [Color figure can be viewed at wileyonlinelibrary.com]

4 | DISCUSSION

In this study we have defined the polyadenylated transcriptome of nm-cSCs from the central portion of the naïve adult rabbit cornea. To our knowledge, this is the first report characterizing cSCs from any mammalian species, as neither mouse (Kaplan et al., 2019) nor human (Collin et al., 2020) scRNA-seq analyses have reported on these glial cells of the cornea. Here, we showed that nm-cSCs of adult corneas transcribe, and translate genes of major conserved protein markers that reflect their SC lineage, contrary to a previous study reporting expression of some mRNAs of mature SCs, but fail to translate these transcripts into proteins in the embryonic corneas of chick (Conrad et al., 2009). It would be of future interest to know how cSC genes are regulated postnatally at eye opening and into early adulthood (1 month of age), the periods during which corneal nerves undergo extensive physiological remodeling (Wang et al., 2012).

Our data illuminate key protein biomarkers useful to the study of nm-cSCs and unveil insights into novel corneal transcripts. L1CAM is involved in cell–cell interactions between axon pairs, as well as between axons and SCs (Schmid et al., 2000). L1CAM-deficient mice show improved axon sprouting and regeneration through increased SC proliferation (Guseva et al., 2009); this target may also be implicated in corneal injury repair (Stepp, Pal-Ghosh, Tadvalkar, Li, et al., 2018). Because nm-cSCs from the central cornea of rabbit did not express *L1CAM* transcripts, but the protein is clearly expressed in mouse cornea, it appears that the *L1CAM* gene may be regulated in a species-related manner in the cornea.

We were surprised to find *MPZ* transcripts in the nm-cSCs, because conventionally, MPZ is accepted as marker of m-SCs (Sock & Wegner, 2019). However, our findings are not unique; *MPZ* transcripts were also noted in transcriptomic studies of human choroid samples, revealing low levels of *MPZ* expression in nm-SCs of this tissue (Voigt et al., 2019). Similarly, low levels of *MAL* transcripts were also found in the rabbit nm-cSCs. Considering that myelin-related genes are regulated through transcriptional activity of SOX10 (Jessen & Mirsky, 2002; Sock & Wegner, 2019), which was co-expressed in nm-cSCs, we speculate that *MPZ* and *MAL* transcripts may be potentially blocked from translation in these cells. This contention is supported by the localization of MPZ in m-cSCs of the peripheral cornea and its absence in nm-cSCs of the central cornea.

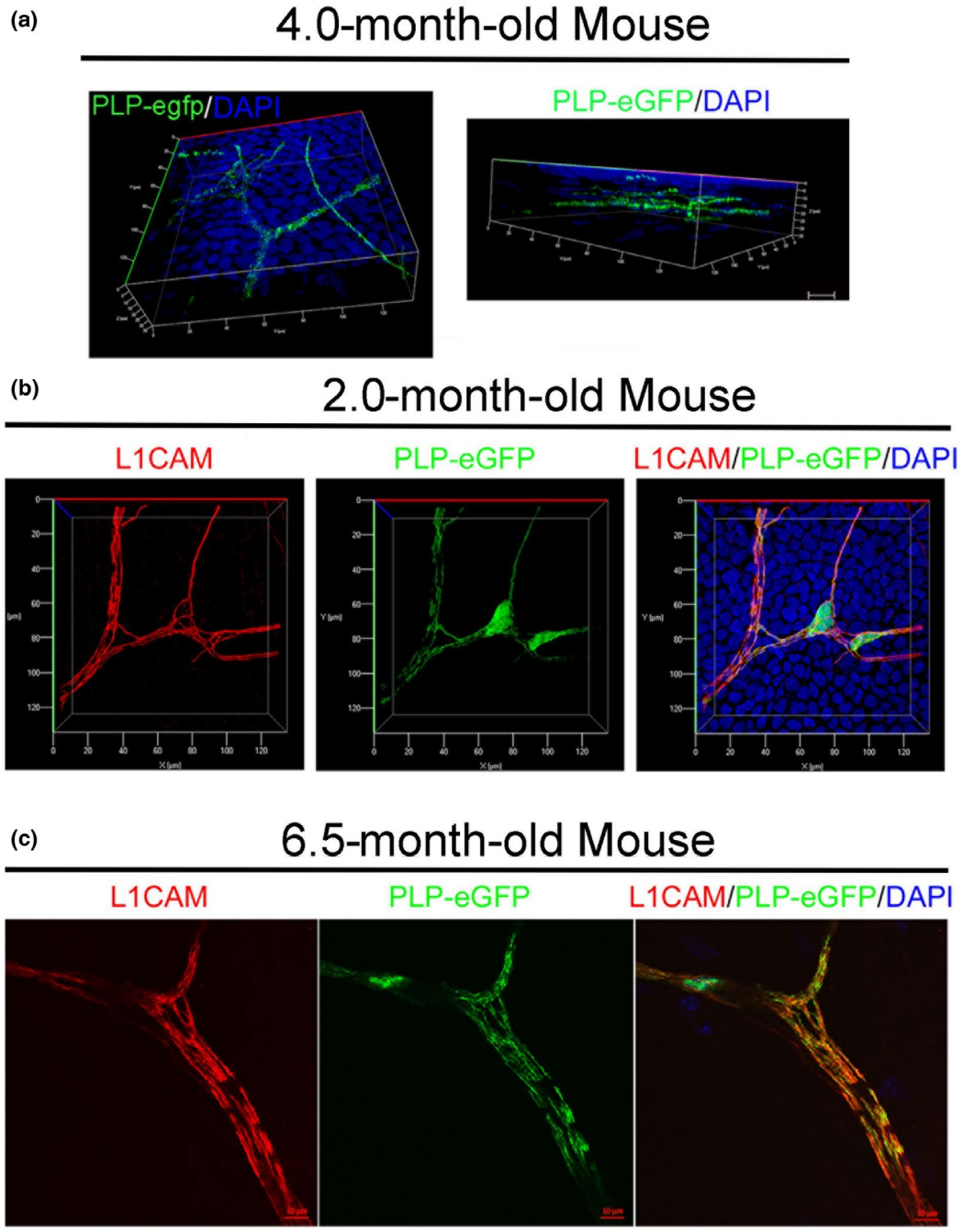

FIGURE 10 Plp1 gene promoter drives reporter gene expression in cSCs. Corneas ($n = 3$ for each age) from transgenic*Plp1*-eGFP mice were collected at different ages (2 M, 4 M, and 6.5 M), and processed for whole-mount immunohistochemistry. Some samples were co-immunostained for L1CAM (*red*). (a) Representative 3D reconstructions at different orientations of 35 μmz-stacks acquired in the central portion of the cornea of 4-M-old*Plp1*-eGFP transgenic mouse. (b)*En face*3D reconstruction ofz-stacks acquired in the central portion of the corneal stroma of 2-M-old*Plp1*-eGFP transgenic mouse; nm-cSCs were co-stained for L1CAM (*red*). (c) Confocalz-stacks acquired in the central portion of the corneal stroma of 6.5-M-old*Plp1*-eGFP co-immunostained for L1CAM (*red*). Strong co-localization between L1CAM (*red*) and eGFP (*green*) was noted. Nuclei were stained with DAPI (*blue*). All images were taken at 63× magnification; Scale bars, 10 μm. eGFP = enhanced green fluorescent protein [Color figure can be viewed at wileyonlinelibrary.com]

Further insights into this conundrum come from recent findings that certain genes previously assigned to the function of myelination are more highly expressed in nm-SCs than in m-SCs; these authors speculate that these "myelination" mRNAs could play other novel roles in nm-SCs (Wolbert et al., 2020).

SCN7A belongs to the family of voltage-gated "glial" sodium channels that sustain the generation and propagation of electrical activity in excitable tissues (Widenfalk et al., 1998). SCN7A could possibly play a role in Na^+ electrolyte balance to support corneal hydration through regulation of tear osmolality, which would be

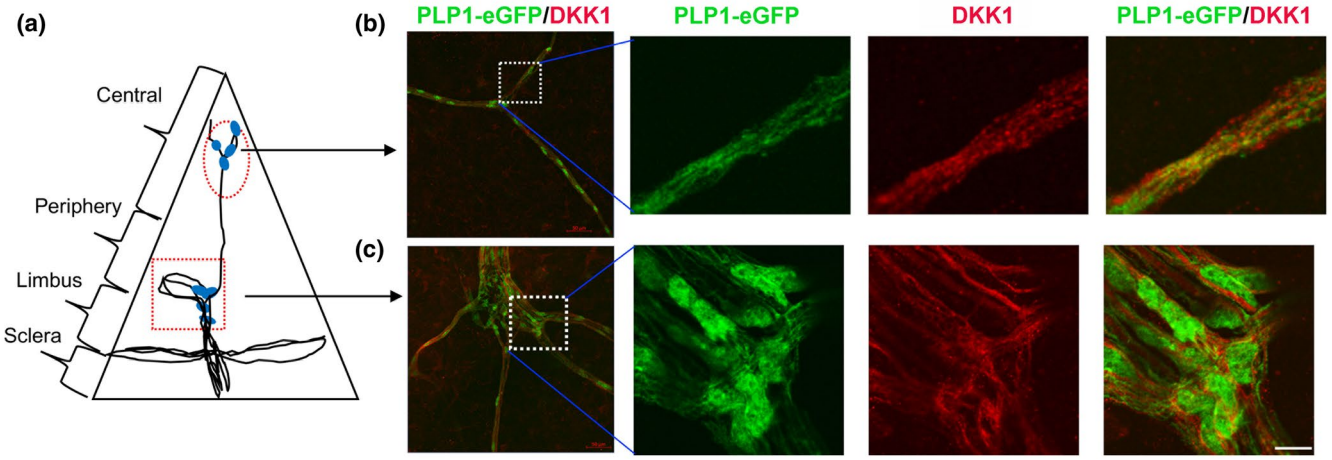

FIGURE 11 Visualization of DKK1 expression in cSCs in the Plp1-eGFP mouse cornea. (a) Schematic representation of the cornea mapping the distribution of stromal axons and cSCs. Representative confocal images of stromal axons immunostained for DKK1 (*red*) ($n = 3$) shown in panel (b) are from the central cornea (a,*dotted circle)*, and in panel c from the limbal/peripheral area (a,*dotted rectangle*).*Dotted rectangles*in panels b and c: images of stromal nm-cSCs were manually enlarged 3×. Note that DKK1$^+$cells co-localized with eGFP in both the central and peripheral regions of the cornea. Scale bars, 10 μm [Color figure can be viewed at wileyonlinelibrary.com]

relevant to dry eye syndrome (Dartt, 2009; Liu et al., 2009; Potvin et al., 2015). GFRA3 belongs to the glial cell line-derived neurotrophic factor (GDNF) family of cell surface receptors (Watanabe et al., 2002). As a survival factor for PNS neurons, GFRA3 associates with the RET tyrosine kinase (Schlee et al., 2006) to support axonal regeneration (Wong et al., 2015). We found *GFRA3*$^+$ nm-cSCs on stromal axons but not in the subbasal counterparts, suggesting this compartmentalized distribution could potentially result in differences in how these particular axons respond to trophic factors during an injury. Syndecans are a major family of cell surface heparan sulfate proteoglycans known to be expressed in the cornea (Stepp et al., 2015). SDC3 is expressed in both axons and SCs (Chernousov et al., 1996), and because SDC3, a non-RET receptor, also binds to GDNF members (Bespalov et al., 2011), this potentially implicates overlapping roles for SDC3 with GFRA3 in cSC functions. Future biochemical studies to unravel their functional roles will need to be done.

The WNT inhibitor DKK1 may have an important cornea-specific role in SCs, given that other PNS tissues do not express this gene in SCs from interrogation of literature and the *PanglaoDB* (Arthur-Farraj et al., 2012; Franzen et al., 2019; Monje et al., 2018; Wolbert et al., 2020), and *Harmonizome* databases (Rouillard et al., 2016). A search for the transcripts for the DKK1 co-receptors *LRP5/6* (Niehrs, 2006) in the rabbit nm-cSCs transcriptome revealed these were absent, alluding to other stromal cell types that may be the target of this secreted factor. Potentially DKK1 is secreted by cSCs and binds to its receptor on axons (Tawk et al., 2011), or alternatively, on another corneal cell type, where it can exert its inhibition of WNT signaling. It remains to be shown how SC-derived DKK1 regulates corneal sensory function under normal and pathological states.

We were limited in our study by the need to perform SC target validation in mouse corneas, due to the lack of antibodies against rabbit targets. In this respect, the scRNA-seq data are from male rabbits as this sex was available to us, which is a limitation of this study. However, despite this, our strategy allowed us to explore conserved features of the central cornea to profile representative targets in mouse using both sexes. In our immunostaining analysis we did not observe any apparent sex differences. The use of murine models offers numerous advantages, as mice are genetically tractable and widely employed for longitudinal studies related to physiology and experimental injury (Bouheraoua et al., 2019; Namavari et al., 2011). For instance, the *Plp1*-eGFP transgenic line is well-suited for longitudinal studies on nerve injury (Gomez-Sanchez et al., 2017) and has also afforded discovery of novel functions of SCs related to nociception in the dermis (Abdo et al., 2019).

Another growing area of application of scRNA-seq technology is related to anatomy-specific gene expression affording region-specific targets to be illuminated that otherwise may not have been identified from the full tissue. Such studies comparing central with peripheral retina, or similar approaches applied to the cornea, have provided insight also into human ocular diseases (Collin et al., 2020; Voigt et al., 2019). Although DKK1 does not appear specific to the central corneal nm-cSCs, a number of additional nm-cSC genes we identified now remain to be validated and functionally characterized. The rabbit nm-cSC transcriptome thus serves as a starting point for such comparative transcriptomics for future explorations.

DECLARATION OF TRANSPARENCY

The authors, reviewers and editors affirm that in accordance to the policies set by the *Journal of Neuroscience Research*, this manuscript presents an accurate and transparent account of the study being reported and that all critical details describing the methods and results are present.

ACKNOWLEDGMENTS

We thank Maya Yankova at the UConn Health Electron Microscopy Core facility, Susan Staurovsky from the CCAM Microscopy Facility at UConn Health, and Diane Luo and Dr. Michael Samuels from the Single Cell Biology Service at JAX for their technical assistance.

CONFLICT OF INTEREST

The authors have no conflict of interest.

AUTHOR CONTRIBUTIONS

All the authors had access to the data in the study and take responsibility for the integrity and the accuracy of the data analysis. *Conceptualization*, P.B.M. and R.M.; *Methodology*, P.B.M., G.S., B.R., S.P.G., K.S.G., P.R. and R.M.; *Software*, B.R., E.F.T. and P.R.; *Validation*, P.B.M., B.R., P.R. and R.M.; *Investigation*, P.B.M., B.R., P.R., K.S.G., S.P.G. and R.M.; *Formal Analysis*, P.B.M., G.S., B.R., M.A.S., P.R., S.P.G., W.B.M. and R.M.; *Resources*, P.B.M., B.R., E.F.T., M.A.S., W.B.M., P.R. and R.M.; *Writing – Original Draft*, P.B.M. and R.M.; *Writing – Review & Editing*, P.B.M., G.S., B.R., E.F.T., M.A.S., W.B.M, P.R. and R.M.; *Visualization*, P.B.M., B.R., S.P.G., M.A.S., P.R. and R.M.; *Supervision*, P.B.M., E.F.T., M.A.S., W.B.M., P.R. and R.M.; *Project Management*, P.B.M., E.F.T., M.A.S., W.B.M., P.R. and R.M.; *Funding Acquisition*, P.B.M., E.F.T., M.A.S., W.B.M., P.R. and R.M.

PEER REVIEW

The peer review history for this article is available at https://publons.com/publon/10.1002/jnr.24757.

DATA AVAILABILITY STATEMENT

The nm-cSC raw data will become available through the NCBI GEO accession number GSE161487.

ORCID

Ephraim F. Trakhtenberg https://orcid.org/0000-0003-2844-4191
Paul Robson https://orcid.org/0000-0002-0191-3958
Royce Mohan https://orcid.org/0000-0002-5102-0437

REFERENCES

Abdo, H., Calvo-Enrique, L., Lopez, J. M., Song, J., Zhang, M.-D., Usoskin, D., El Manira, A., Adameyko, I., Hjerling-Leffler, J., & Ernfors, P. (2019). Specialized cutaneous Schwann cells initiate pain sensation. *Science*, *365*(6454), 695–699. https://doi.org/10.1126/science.aax6452

Ahn, V. E., Chu, M. L., Choi, H. J., Tran, D., Abo, A., & Weis, W. I. (2011). Structural basis of Wnt signaling inhibition by Dickkopf binding to LRP5/6. *Developmental Cell*, *21*(5), 862–873. https://doi.org/10.1016/j.devcel.2011.09.003

Al-Aqaba, M. A., Fares, U., Suleman, H., Lowe, J., & Dua, H. S. (2010). Architecture and distribution of human corneal nerves. *British Journal of Ophthalmology*, *94*(6), 784–789. https://doi.org/10.1136/bjo.2009.173799

Arthur-Farraj, P. J., Latouche, M., Wilton, D. K., Quintes, S., Chabrol, E., Banerjee, A., Woodhoo, A., Jenkins, B., Rahman, M., Turmaine, M., Wicher, G. K., Mitter, R., Greensmith, L., Behrens, A., Raivich, G., Mirsky, R., & Jessen, K. R. (2012). c-Jun reprograms Schwann cells of injured nerves to generate a repair cell essential for regeneration. *Neuron*, *75*(4), 633–647. https://doi.org/10.1016/j.neuron.2012.06.021

Arthur-Farraj, P. J., Morgan, C. C., Adamowicz, M., Gomez-Sanchez, J. A., Fazal, S. V., Beucher, A., Razzaghi, B., Mirsky, R., Jessen, K. R., & Aitman, T. J. (2017). Changes in the Coding and non-coding transcriptome and DNA methylome that define the Schwann cell repair phenotype after nerve injury. *Cell Reports*, *20*(11), 2719–2734. https://doi.org/10.1016/j.celrep.2017.08.064

Bargagna-Mohan, P., Ishii, A., Lei, L., Sheehy, D., Pandit, S., Chan, G., Bansal, R., & Mohan, R. (2017). Sustained activation of ERK1/2 MAPK in Schwann cells causes corneal neurofibroma. *Journal of Neuroscience Research*, *95*(9), 1712–1729. https://doi.org/10.1002/jnr.24067

Benson, M. D., Khor, C. C., Gage, P. J., & Lehmann, O. J. (2017). A targeted approach to genome-wide studies reveals new genetic associations with central corneal thickness. *Molecular Vision*, *23*, 952–962. https://www.ncbi.nlm.nih.gov/pubmed/29296075

Bespalov, M. M., Sidorova, Y. A., Tumova, S., Ahonen-Bishopp, A., Magalhães, A. C., Kulesskiy, E., Paveliev, M., Rivera, C., Rauvala, H., & Saarma, M. (2011). Heparan sulfate proteoglycan syndecan-3 is a novel receptor for GDNF, neurturin, and artemin. *Journal of Cell Biology*, *192*(1), 153–169. https://doi.org/10.1083/jcb.201009136

Bi, L., & Lwigale, P. (2019). Transcriptomic analysis of differential gene expression during chick periocular neural crest differentiation into corneal cells. *Developmental Dynamics*, *248*(7), 583–602. https://doi.org/10.1002/dvdy.43

Blake, J. A., & Ziman, M. R. (2013). The characterisation of Pax3 expressant cells in adult peripheral nerve. *PLoS One*, *8*(3), e59184. https://doi.org/10.1371/journal.pone.0059184

Bouheraoua, N., Fouquet, S., Marcos-Almaraz, M. T., Karagogeos, D., Laroche, L., & Chedotal, A. (2019). Genetic analysis of the organization, development, and plasticity of corneal innervation in mice. *Journal of Neuroscience*, *39*(7), 1150–1168. https://doi.org/10.1523/JNEUROSCI.1401-18.2018

Bremer, M., Frob, F., Kichko, T., Reeh, P., Tamm, E. R., Suter, U., & Wegner, M. (2011). Sox10 is required for Schwann-cell homeostasis and myelin maintenance in the adult peripheral nerve. *Glia*, *59*(7), 1022–1032. https://doi.org/10.1002/glia.21173

Buchstaller, J., Sommer, L., Bodmer, M., Hoffmann, R., Suter, U., & Mantei, N. (2004). Efficient isolation and gene expression profiling of small numbers of neural crest stem cells and developing Schwann cells. *Journal of Neuroscience*, *24*(10), 2357–2365. https://doi.org/10.1523/JNEUROSCI.4083-03.2004

Chernousov, M. A., Stahl, R. C., & Carey, D. J. (1996). Schwann cells secrete a novel collagen-like adhesive protein that binds N-syndecan. *Journal of Biological Chemistry*, *271*(23), 13844–13853. https://doi.org/10.1074/jbc.271.23.13844

Chng, Z., Peh, G. S. L., Herath, W. B., Cheng, T. Y. D., Ang, H.-P., Toh, K.-P., Robson, P., Mehta, J. S., & Colman, A. (2013). High throughput gene expression analysis identifies reliable expression markers of human corneal endothelial cells. *PLoS One*, *8*(7), e67546. https://doi.org/10.1371/journal.pone.0067546

Clements, M. P., Byrne, E., Camarillo Guerrero, L. F., Cattin, A.-L., Zakka, L., Ashraf, A., Burden, J. J., Khadayate, S., Lloyd, A. C., Marguerat, S., & Parrinello, S. (2017). The wound microenvironment reprograms Schwann cells to invasive mesenchymal-like cells to drive peripheral nerve regeneration. *Neuron*, *96*(1), 98–114.e7. https://doi.org/10.1016/j.neuron.2017.09.008

Collin, J., Queen, R., Zerti, D., Bojic, S., Moyse, N., Molina, M. M., Yang, C., Reynolds, G., Hussain, R., Coxhead, J. M., Lisgo, S., Henderson, D., Joseph, A., Rooney, P., Ghosh, S., Cannon, C., Haniffa, M., Figueiredo, F., Armstrong, L., & Lako, M. (2020). A single cell atlas of human

cornea that defines its development, limbal stem and progenitor cells and the interactions with the limbal niche. *BioRxiv*, 1–43. https://doi.org/10.1101/2020.07.09.195438

Conrad, A. H., Albrecht, M., Pettit-Scott, M., & Conrad, G. W. (2009). Embryonic corneal Schwann cells express some Schwann cell marker mRNAs, but no mature Schwann cell marker proteins. *Investigative Ophthalmology & Visual Science*, *50*(9), 4173–4184. https://doi.org/10.1167/iovs.08-3136

Dartt, D. A. (2009). Neural regulation of lacrimal gland secretory processes: Relevance in dry eye diseases. *Progress in Retinal and Eye Research*, *28*(3), 155–177. https://doi.org/10.1016/j.preteyeres.2009.04.003

Feltri, M. L., Poitelon, Y., & Previtali, S. C. (2016). How Schwann cells sort axons: New concepts. *Neuroscientist*, *22*(3), 252–265. https://doi.org/10.1177/1073858415572361

Fini, M. E., Cook, J. R., & Mohan, R. (1998). Proteolytic mechanisms in corneal ulceration and repair. *Archives of Dermatological Research*, *290*(Suppl), S12–S23. https://doi.org/10.1007/PL00007449

Fini, M. E., & Stramer, B. M. (2005). How the cornea heals: Cornea-specific repair mechanisms affecting surgical outcomes. *Cornea*, *24*(8 Suppl), S2–S11. https://www.ncbi.nlm.nih.gov/pubmed/16227819

Franzen, O., Gan, L. M., & Bjorkegren, J. L. M. (2019). PanglaoDB: A web server for exploration of mouse and human single-cell RNA sequencing data. *Database*, *2019*. https://doi.org/10.1093/database/baz046

Geisert, E. E., Lu, L., Freeman-Anderson, N. E., Templeton, J. P., Nassr, M., Wang, X., & Williams, R. W. (2009). Gene expression in the mouse eye: An online resource for genetics using 103 strains of mice. *Molecular Vision*, *15*, 1730–1763. https://www.ncbi.nlm.nih.gov/pubmed/19727342

Gomez-Sanchez, J. A., Pilch, K. S., van der Lans, M., Fazal, S. V., Benito, C., Wagstaff, L. J., Mirsky, R., & Jessen, K. R. (2017). After nerve injury, lineage tracing shows that myelin and Remak Schwann cells elongate extensively and branch to form repair Schwann cells, which shorten radically on remyelination. *Journal of Neuroscience*, *37*(37), 9086–9099. https://doi.org/10.1523/JNEUROSCI.1453-17.2017

Guerrero-Juarez, C. F., Dedhia, P. H., Jin, S., Ruiz-Vega, R., Ma, D., Liu, Y., Yamaga, K., Shestova, O., Gay, D. L., Yang, Z., Kessenbrock, K., Nie, Q., Pear, W. S., Cotsarelis, G., & Plikus, M. V. (2019). Single-cell analysis reveals fibroblast heterogeneity and myeloid-derived adipocyte progenitors in murine skin wounds. *Nature Communications*, *10*(1), 650. https://doi.org/10.1038/s41467-018-08247-x

Guseva, D., Angelov, D. N., Irintchev, A., & Schachner, M. (2009). Ablation of adhesion molecule L1 in mice favours Schwann cell proliferation and functional recovery after peripheral nerve injury. *Brain*, *132*(Pt 8), 2180–2195. https://doi.org/10.1093/brain/awp160

Harty, B. L., & Monk, K. R. (2017). Unwrapping the unappreciated: Recent progress in Remak Schwann cell biology. *Current Opinion in Neurobiology*, *47*, 131–137. https://doi.org/10.1016/j.conb.2017.10.003

He, J., & Bazan, H. E. (2016). Neuroanatomy and neurochemistry of mouse cornea. *Investigative Ophthalmology & Visual Science*, *57*(2), 664–674. https://doi.org/10.1167/iovs.15-18019

Jessen, K. R., & Mirsky, R. (2002). Signals that determine Schwann cell identity. *Journal of Anatomy*, *200*(4), 367–376. https://doi.org/10.1046/j.1469-7580.2002.00046.x

Jessen, K. R., & Mirsky, R. (2016). The repair Schwann cell and its function in regenerating nerves. *Journal of Physiology*, *594*(13), 3521–3531. https://doi.org/10.1113/JP270874

Jessen, K. R., Mirsky, R., & Lloyd, A. C. (2015). Schwann cells: Development and role in nerve repair. *Cold Spring Harbor Perspectives in Biology*, *7*(7), a020487. https://doi.org/10.1101/cshperspect.a020487

Jessen, K. R., Mirsky, R., & Salzer, J. (2008). Introduction. Schwann cell biology. *Glia*, *56*(14), 1479–1480. https://doi.org/10.1002/glia.20779

Jindal, A., Gupta, P., Jayadeva, & Sengupta, D. (2018). Discovery of rare cells from voluminous single cell expression data. *Nature Communications*, *9*(1), 4719. https://doi.org/10.1038/s41467-018-07234-6

Kaplan, N., Wang, J., Wray, B., Patel, P., Yang, W., Peng, H., & Lavker, R. M. (2019). Single-cell RNA transcriptome helps define the limbal/corneal epithelial stem/early transit amplifying cells and how autophagy affects this population. *Investigative Ophthalmology & Visual Science*, *60*(10), 3570–3583. https://doi.org/10.1167/iovs.19-27656

Lieven, O., & Ruther, U. (2011). The Dkk1 dose is critical for eye development. *Developmental Biology*, *355*(1), 124–137. https://doi.org/10.1016/j.ydbio.2011.04.023

Liu, H., Begley, C., Chen, M., Bradley, A., Bonanno, J., McNamara, N. A., Nelson, J. D., & Simpson, T. (2009). A link between tear instability and hyperosmolarity in dry eye. *Investigative Ophthalmology & Visual Science*, *50*(8), 3671–3679. https://doi.org/10.1167/iovs.08-2689

Mallon, B. S., Shick, H. E., Kidd, G. J., & Macklin, W. B. (2002). Proteolipid promoter activity distinguishes two populations of NG2-positive cells throughout neonatal cortical development. *Journal of Neuroscience*, *22*(3), 876–885. https://www.ncbi.nlm.nih.gov/pubmed/11826117

Mickelsen, L. E., Bolisetty, M., Chimileski, B. R., Fujita, A., Beltrami, E. J., Costanzo, J. T., Naparstek, J. R., Robson, P., & Jackson, A. C. (2019). Single-cell transcriptomic analysis of the lateral hypothalamic area reveals molecularly distinct populations of inhibitory and excitatory neurons. *Nature Neuroscience*, *22*(4), 642–656. https://doi.org/10.1038/s41593-019-0349-8

Mimura, T., Amano, S., Yokoo, S., Uchida, S., Usui, T., & Yamagami, S. (2008). Isolation and distribution of rabbit keratocyte precursors. *Molecular Vision*, *14*, 197–203. https://www.ncbi.nlm.nih.gov/pubmed/18334932

Monje, P. V., Sant, D., & Wang, G. (2018). Phenotypic and functional characteristics of human Schwann cells as revealed by cell-based assays and RNA-SEQ. *Molecular Neurobiology*, *55*(8), 6637–6660. https://doi.org/10.1007/s12035-017-0837-3

Muller, L. J., Marfurt, C. F., Kruse, F., & Tervo, T. M. (2003). Corneal nerves: Structure, contents and function. *Experimental Eye Research*, *76*(5), 521–542. https://www.ncbi.nlm.nih.gov/pubmed/12697417

Muller, L. J., Pels, L., & Vrensen, G. F. (1996). Ultrastructural organization of human corneal nerves. *Investigative Ophthalmology & Visual Science*, *37*(4), 476–488. https://www.ncbi.nlm.nih.gov/pubmed/8595948

Nakatsu, M. N., Ding, Z., Ng, M. Y., Truong, T. T., Yu, F., & Deng, S. X. (2011). Wnt/beta-catenin signaling regulates proliferation of human cornea epithelial stem/progenitor cells. *Investigative Ophthalmology & Visual Science*, *52*(7), 4734–4741. https://doi.org/10.1167/iovs.10-6486

Namavari, A., Chaudhary, S., Sarkar, J., Yco, L., Patel, K., Han, K. Y., Yue, B. Y., Chang, J.-H., & Jain, S. (2011). In vivo serial imaging of regenerating corneal nerves after surgical transection in transgenic thy1-YFP mice. *Investigative Ophthalmology & Visual Science*, *52*(11), 8025–8032. https://doi.org/10.1167/iovs.11-8332

Napoli, I., Noon, L. A., Ribeiro, S., Kerai, A. P., Parrinello, S., Rosenberg, L. H., & Lloyd, A. C. (2012). A central role for the ERK-signaling pathway in controlling Schwann cell plasticity and peripheral nerve regeneration in vivo. *Neuron*, *73*(4), 729–742. https://doi.org/10.1016/j.neuron.2011.11.031

Niehrs, C. (2006). Function and biological roles of the Dickkopf family of Wnt modulators. *Oncogene*, *25*(57), 7469–7481. https://doi.org/10.1038/sj.onc.1210054

Ojeda, J. L., Ventosa, J. A., & Piedra, S. (2001). The three-dimensional microanatomy of the rabbit and human cornea. A chemical and mechanical microdissection-SEM approach. *Journal of Anatomy*, *199*(Pt 5), 567–576. https://doi.org/10.1046/j.1469-7580.2001.19950567.x

Pal-Ghosh, S., Tadvalkar, G., & Stepp, M. A. (2017). Alterations in corneal sensory nerves during homeostasis, aging, and after injury in mice lacking the heparan sulfate proteoglycan syndecan-1. *Investigative Ophthalmology & Visual Science*, *58*(12), 4959–4975. https://doi.org/10.1167/iovs.17-21531

Potvin, R., Makari, S., & Rapuano, C. J. (2015). Tear film osmolarity and dry eye disease: A review of the literature. *Clinical Ophthalmology*, *9*, 2039–2047. https://doi.org/10.2147/OPTH.S95242

Qiu, X., Hill, A., Packer, J., Lin, D., Ma, Y. A., & Trapnell, C. (2017). Single-cell mRNA quantification and differential analysis with Census. *Nature Methods*, *14*(3), 309–315. https://doi.org/10.1038/nmeth.4150

Qiu, X., Mao, Q., Tang, Y., Wang, L., Chawla, R., Pliner, H. A., & Trapnell, C. (2017). Reversed graph embedding resolves complex single-cell trajectories. *Nature Methods*, *14*(10), 979–982. https://doi.org/10.1038/nmeth.4402

Rheaume, B. A., Jereen, A., Bolisetty, M., Sajid, M. S., Yang, Y., Renna, K., Sun, L., Robson, P., & Trakhtenberg, E. F. (2018). Single cell transcriptome profiling of retinal ganglion cells identifies cellular subtypes. *Nature Communications*, *9*(1), 2759. https://doi.org/10.1038/s41467-018-05134-3

Rouillard, A. D., Gundersen, G. W., Fernandez, N. F., Wang, Z., Monteiro, C. D., McDermott, M. G., & Ma'ayan, A. (2016). The harmonizome: A collection of processed datasets gathered to serve and mine knowledge about genes and proteins. *Database*, *2016*, 1–16. https://doi.org/10.1093/database/baw100

Schlee, S., Carmillo, P., & Whitty, A. (2006). Quantitative analysis of the activation mechanism of the multicomponent growth-factor receptor Ret. *Nature Chemical Biology*, *2*(11), 636–644. https://doi.org/10.1038/nchembio823

Schmid, R. S., Pruitt, W. M., & Maness, P. F. (2000). A MAP kinase-signaling pathway mediates neurite outgrowth on L1 and requires Src-dependent endocytosis. *Journal of Neuroscience*, *20*(11), 4177–4188. https://www.ncbi.nlm.nih.gov/pubmed/10818153

Shaheen, B. S., Bakir, M., & Jain, S. (2014). Corneal nerves in health and disease. *Survey of Ophthalmology*, *59*(3), 263–285. https://doi.org/10.1016/j.survophthal.2013.09.002

Sock, E., & Wegner, M. (2019). Transcriptional control of myelination and remyelination. *Glia*, *67*(11), 2153–2165. https://doi.org/10.1002/glia.23636

Stepp, M. A., Pal-Ghosh, S., Tadvalkar, G., Li, L., Brooks, S. R., & Morasso, M. I. (2018). Molecular basis of Mitomycin C enhanced corneal sensory nerve repair after debridement wounding. *Scientific Reports*, *8*(1), 16960. https://doi.org/10.1038/s41598-018-35090-3

Stepp, M. A., Pal-Ghosh, S., Tadvalkar, G., & Pajoohesh-Ganji, A. (2015). Syndecan-1 and its expanding list of contacts. *Advances in Wound Care*, *4*(4), 235–249. https://doi.org/10.1089/wound.2014.0555

Stepp, M. A., Pal-Ghosh, S., Tadvalkar, G., Williams, A., Pflugfelder, S. C., & de Paiva, C. S. (2018). Reduced intraepithelial corneal nerve density and sensitivity accompany desiccating stress and aging in C57BL/6 mice. *Experimental Eye Research*, *169*, 91–98. https://doi.org/10.1016/j.exer.2018.01.024

Stepp, M. A., Tadvalkar, G., Hakh, R., & Pal-Ghosh, S. (2017). Corneal epithelial cells function as surrogate Schwann cells for their sensory nerves. *Glia*, *65*(6), 851–863. https://doi.org/10.1002/glia.23102

Tawk, M., Makoukji, J., Belle, M., Fonte, C., Trousson, A., Hawkins, T., & Massaad, C. (2011). Wnt/beta-catenin signaling is an essential and direct driver of myelin gene expression and myelinogenesis. *Journal of Neuroscience*, *31*(10), 3729–3742. https://doi.org/10.1523/JNEUROSCI.4270-10.2011

Trapnell, C., Cacchiarelli, D., Grimsby, J., Pokharel, P., Li, S., Morse, M., Lennon, N. J., Livak, K. J., Mikkelsen, T. S., & Rinn, J. L. (2014). The dynamics and regulators of cell fate decisions are revealed by pseudotemporal ordering of single cells. *Nature Biotechnology*, *32*(4), 381–386. https://doi.org/10.1038/nbt.2859

Voigt, A. P., Mulfaul, K., Mullin, N. K., Flamme-Wiese, M. J., Giacalone, J. C., Stone, E. M., Tucker, B. A., Scheetz, T. E., & Mullins, R. F. (2019). Single-cell transcriptomics of the human retinal pigment epithelium and choroid in health and macular degeneration. *Proceedings of the National Academy of Sciences of the United States of America*, *116*(48), 24100–24107. https://doi.org/10.1073/pnas.1914143116

Wang, C., Fu, T., Xia, C., & Li, Z. (2012). Changes in mouse corneal epithelial innervation with age. *Investigative Ophthalmology & Visual Science*, *53*(8), 5077–5084. https://doi.org/10.1167/iovs.12-9704

Watanabe, E., Hiyama, T. Y., Kodama, R., & Noda, M. (2002). NaX sodium channel is expressed in non-myelinating Schwann cells and alveolar type II cells in mice. *Neuroscience Letters*, *330*(1), 109–113. https://doi.org/10.1016/s0304-3940(02)00708-5

Widenfalk, J., Tomac, A., Lindqvist, E., Hoffer, B., & Olson, L. (1998). GFRalpha-3, a protein related to GFRalpha-1, is expressed in developing peripheral neurons and ensheathing cells. *European Journal of Neuroscience*, *10*(4), 1508–1517. https://doi.org/10.1046/j.1460-9568.1998.00192.x

Wight, P. A., Duchala, C. S., Readhead, C., & Macklin, W. B. (1993). A myelin proteolipid protein-LacZ fusion protein is developmentally regulated and targeted to the myelin membrane in transgenic mice. *Journal of Cell Biology*, *123*(2), 443–454. https://doi.org/10.1083/jcb.123.2.443

Wolbert, J., Li, X., Heming, M., Mausberg, A. K., Akkermann, D., Frydrychowicz, C., Fledrich, R., Groeneweg, L., Schulz, C., Stettner, M., Alonso Gonzalez, N., Wiendl, H., Stassart, R., & Meyer zu Hörste, G. (2020). Redefining the heterogeneity of peripheral nerve cells in health and autoimmunity. *Proceedings of the National Academy of Sciences of the United States of America*, *117*(17), 9466–9476. https://doi.org/10.1073/pnas.1912139117

Wong, L. E., Gibson, M. E., Arnold, H. M., Pepinsky, B., & Frank, E. (2015). Artemin promotes functional long-distance axonal regeneration to the brainstem after dorsal root crush. *Proceedings of the National Academy of Sciences of the United States of America*, *112*(19), 6170–6175. https://doi.org/10.1073/pnas.1502057112

Yang, A. Y., Chow, J., & Liu, J. (2018). Corneal innervation and sensation: The eye and beyond. *Yale Journal of Biology and Medicine*, *91*(1), 13–21. https://www.ncbi.nlm.nih.gov/pubmed/29599653

You, J., Corley, S. M., Wen, L. I., Hodge, C., Höllhumer, R., Madigan, M. C., Wilkins, M. R., & Sutton, G. (2018). RNA-Seq analysis and comparison of corneal epithelium in keratoconus and myopia patients. *Scientific Reports*, *8*(1), 389. https://doi.org/10.1038/s41598-017-18480-x

Zheng, G. X. Y., Terry, J. M., Belgrader, P., Ryvkin, P., Bent, Z. W., Wilson, R., Ziraldo, S. B., Wheeler, T. D., McDermott, G. P., Zhu, J., Gregory, M. T., Shuga, J., Montesclaros, L., Underwood, J. G., Masquelier, D. A., Nishimura, S. Y., Schnall-Levin, M., Wyatt, P. W., Hindson, C. M., … Bielas, J. H. (2017). Massively parallel digital transcriptional profiling of single cells. *Nature Communications*, *8*, 14049. https://doi.org/10.1038/ncomms14049

SUPPORTING INFORMATION

Additional supporting information may be found online in the Supporting Information section.

FIGURE S1 Quality control. The distributions of corneal cells were used to identify outliers and apply thresholds. The upper panel is a histogram which highlights the distribution of UMIs (green) and genes (blue). This histogram was used to set the threshold for initial quality control by identifying outlier peaks. The red bar represent the thresholds for cutoffs: cells needed to have >2,000 UMIs and >800 genes for inclusion. The dot plot of cells in the lower panel shows the number of UMIs vs the number of genes detected. Red cells are those that fail the inclusion criteria and black cells are those that have passed

FIGURE S2 Principal component analysis (PCA). Elbow plot showing the relationship between the number of principal components (PCs) and the amount of variance explained by each component. The

"elbow" of the plot was identified as being 12 PCs (black arrow), and this was the number of components used for downstream analysis

FIGURE S3 Visualization of m-cSCs in the corneal stroma. (a) Schematic representation of the cornea mapping the distribution of stromal axons and cSCs. Orthogonal view from different planes (*x*/*y*, *x*/*z*, or *y*/*z*) of merged confocal images of corneas ($n = 4$) immunostained for L1CAM (*red*), MPZ or MPB (*green*) were taken in panel b from the central cornea (*dotted circle*), and in panels c and d at the limbal/peripheral area (*dotted rectangle*). To be noted in panel b, the absence of MPZ^+ cells. *Asterisks* in panels c and d demark the nucleus of $L1CAM^+$ cells, and *caret* demarks the nucleus of MPZ^+ cells. Nuclei were stained with DAPI (*blue*). All images were taken at 63× magnification. L1 = L1CAM; MBP = Myelin basic protein; MPZ = Myelin protein zero. $n = 4$ corneas

FIGURE S4 eGFP reporter gene expression in the cornea at different stromal depths. Corneas ($n = 3$) from 2-month-old transgenic PLP1-eGFP mice were whole-mount immunostained for L1CAM (*red*). Confocal images were tiled together to display the distribution of $L1CAM^+/eGFP^+$ nm-cSCs at different depths in the anterior corneal stroma (a), mid stroma (b), and mid-to-posterior stroma (c). All images were taken at 20× magnification; Scale bars, 200 μm. PLP1 = proteolipid protein 1; eGFP = enhanced green fluorescent protein

FIGURE S5 eGFP reporter gene expression across the corneal stroma. Corneas ($n = 3$) from 4-month-old transgenic PLP1-eGFP mice were whole-mount immunostained for L1CAM (*red*). Confocal images assembled together showing the distribution of $L1CAM^+/eGFP^+$ nm-cSCs from the central to peripheral cornea (a); scale bar = 105 μm. The enlarged image (b) represents the central cornea in panel a (*dotted rectangle*). The asterisk marks the nucleus, and dotted arrows mark nm-cSCs that show differential staining for L1CAM. scale bar, 10 μm

Transparent Peer Review Report

Transparent Science Questionnaire for Authors

How to cite this article: Bargagna-Mohan P, Schultz G, Rheaume B, et al. Corneal nonmyelinating Schwann cells illuminated by single-cell transcriptomics and visualized by protein biomarkers. *J Neurosci Res*. 2021;99:731–749. https://doi.org/10.1002/jnr.24757